Solar Energy Materials & Solar Cells 116 (2013) 153–170

Contents lists available at SciVerse ScienceDirect

Solar Energy Materials & Solar Cells

journal homepage: www.elsevier.com/locate/solmat

Unified assay of adverse effects from the varied nanoparticle hybrid in polymer–fullerene organic photovoltaics

Yu-Jui Huang [a], Wei-Chun Lo [b], Shun-Wei Liu [a,c], Chao-Han Cheng [d], Chin-Ti Chen [a,b,*], Juen-Kai Wang [d,e,**]

[a] Institute of Chemistry, Academia Sinica, Taipei 11529, Taiwan, ROC
[b] Department of Applied Chemistry, National Chiao Tung University, Hsinchu 30050, Taiwan, ROC
[c] Department of Electronic Engineering, Mingchi University of Technology, New Taipei City 24301, Taiwan, ROC
[d] Center for Condensed Matter Sciences, National Taiwan University, Taipei 10617, Taiwan, ROC
[e] Institute of Atomic and Molecular Science, Academia Sinica, Taipei 10617, Taiwan, ROC

ARTICLE INFO

Article history:
Received 2 January 2013
Received in revised form
25 March 2013
Accepted 25 March 2013
Available online 23 May 2013

Keywords:
Nanoparticle
Hybrid
Polymer solar cell
Organic photovoltaic

ABSTRACT

Nanoparticles (NPs) having different surface capping agent, variant electrical conductivity and sunlight absorption have been studied for the ternary hybrid containing poly(3-hexylthiophene) (P3HT) and [6,6]-phenyl-C-61-butyric acid methyl ester (PCBM) in bulk heterojunction (BHJ) organic photovoltaics (OPVs). These NPs are composed of conducting gold, semiconducting CdS or PbS, or insulating cage-like molecular silica (POSS). We use a series of microscopic methods including TEM, AFM, SEM, optical, and fluorescence microscopy to estimate NP size and to probe the agglomeration and/or aggregation of NPs in P3HT/PCBM blends. Surface capping agent aromatic thiophenol (SPh) was found to be poor in the dispersion of NPs in P3HT/PCBM blends. The light harvesting of these NPs ranges from transparent (POSS NP), near transparent (CdS NP), visible light absorbing (Au NP), to near-infrared absorbing (PbS NP). Nevertheless, the absorbance of these NPs is all too small relative to that of P3HT polymer. Concerning the charge separation of P3HT exciton, the LUMO energy levels of these NPs have been determined by the combination of optical band-gap energy and HOMO energy levels. By the transient photocurrent time-of-flight method, charge carrier mobility of P3HT/PCBM/NP(CdS-SPh) ternary hybrid was found to be improved, although fluorescence quenching studies imply insufficient or ineffective contact between P3HT and all NPs in the present study. NPs hybrid P3HT/PCBM BHJ OPVs were fabricated by solution process. Regardless of conductivity or sunlight absorbance, all NPs show no improvement on power conversion efficiency of ternary hybrid OPVs, which is 3.03–3.91% less than 4.0–4.1% of P3HT/PCBM OPVs without NPs. Based on the present study, a few problems that associate with the inferior performance of NPs hybrid P3HT/PCBM BHJ OPVs are delineated.

1. Introduction

Polymer-based organic photovoltaics (OPVs), the so called third generation solar cells, provide a potential solar energy utility with favorable features, such as low-cost, all-solution process, large-area, and mechanical flexibility [1–3]. Not long ago, power conversion efficiencies (PCEs) surpassing 5% have been achieved with the blends of poly(3-hexylthiophene) (P3HT) and a fullerene derivative, [6,6]-phenyl-C-61-butyric acid methyl ester (best known as PCBM) [4]. Recently, OPV PCE more than 9% has been realized by renovated device structure and newly developed low-band-gap polymers, which show major absorption wavelength longer than 600 nm and more efficiency in harvesting solar energy [5–18]. Due to the unique structural feature, namely regioregularity, which facilitates the packing of polymer chains, the long wavelength absorption (the vibronic feature in the absorption spectra) of P3HT can be substantially improved by device processing conditions, such as thermal annealing and solvent annealing methods [19–22]. Other than extending absorption wavelength in matching solar spectrum, extensive polymer chain packing often facilitates the photocurrent output of polymer-based bulk heterojunction (BHJ) OPVs because of the favorable active layer nanoscale morphology [23–25], namely interdigitated charge transporting channel (percolation pathway).

In this regard, a wide range of nano-size materials in different forms, such as nanoparticles (NPs), nanocrystals, nanorods, nanofibers, nanoclusters, or quantum dots, have been incorporated into polymer-based OPVs to form the hybrid system [26–28],

* Corresponding author at: Institute of Chemistry, Academia Sinica, Taipei 11529, Taiwan, ROC. Tel.: +886 2 2789 8542; fax: +886 2 2783 1237.
** Corresponding author at: Center for Condensed Matter Sciences, National Taiwan University, Taipei 10617, Taiwan, ROC
E-mail addresses: chintchen@gate.sinica.edu.tw (C.-T. Chen), jkwang@ntu.edu.tw (J.-K. Wang).

0927-0248/$ - see front matter © 2013 Elsevier B.V. All rights reserved.
http://dx.doi.org/10.1016/j.solmat.2013.03.031

which may bring about interdigitated charge transporting channel and thus higher PCE of OPVs can be acquired. These nanomaterials can be electrical conducting (metallic) like Au, Ag, and Pt. They can also be semiconducting, such as CdS, CdSe, CdTe, PbS, PbSe, $CuInSe_2$, ZnO, and TiO_2 [29–31]. Although many of them absorb visible light (such as Ag, Au, CdSe, CdTe, HgTe, and $CuInSe_2$) or near-infrared (IR) light (such as PbS and PbSe), some of them are transparent (such as ZnO and TiO_2) or near transparent (such as Pt NP having no distinct plasmonic resonant absorption or small size CdS NPs) [29–31]. In the ordered organic–inorganic hybrid BHJ OPVs [32], electron transporting inorganic materials (Si, TiO_2, ZnO, CdS, and CdSe) in the form of nanofibers or nanorods are vertically aligned beneath polymer-based active layer on the electrode. However, the PCEs reported for such hybrid solar cells have been modest due to the problem of pore infiltration of the semiconducting polymer into the nanostructures [32–35]. Otherwise, one critical issue of such hybrid polymer-based OPV is the agglomeration and/or aggregation of the nanomaterials if they all blended and solution processed together in the fabrication of BHJ OPVs. Therefore, a surface capping agent or ligand, which is an organic species with an elongated saturated hydrocarbon chain, is implanted onto the surface of these nanomaterials to depress their agglomeration and/or aggregation and to enhance their polymer mixibility.

Here in this report, we are particularly interested in analyzing the impact of organics capped NPs in P3HT/PCBM-based BHJ OPVs, of which the active layer is a ternary hybrid. These NPs are POSS-SC_{16}, CdS-SC_{12}, CdS-SPh, PbS-OA, Au-SC_{12}, and Au-SPh (Scheme 1). In addition to the different surface capping agent, either insulating saturated hydrocarbon chain (SC_{16}, SC_{12}, or OA oleic acid) or semiconducting aromatic benzene ring (SPh), the interior content of these NPs is distinctive in terms of electrical conductivity. They are conducting Au, semiconducting PbS and CdS, and insulating polyhedral oligomeric silsesquioxane (POSS). They are also quite different in sunlight absorption, such as transparent POSS, nearly transparent CdS NP, nearly panchromatic visible light absorption Au NP and near-IR absorption PbS NP. Surveying literature, a broad range of variances in PCE have been reported for NP hybrid P3HT/PCBM BHJ OPVs. A significant improved PCE from 2.63% to 4.08% has been found for conducting Pt NP hybrid OPVs [36]. Similar PCE enhancement (4.08% improved from 3.43%) also has been reported for conducting Ag NP hybrid OPVs [37]. In contrast, no beneficial effect on P3HT/PCBM OPV has been found for conducting Au NP hybrid in a more comprehensive study recently [38], although an earlier report had demonstrated a substantial PCE enhancement for Ag and Au NPs [39]. For semiconducting CdS NP hybrid P3HT/PCBM OPVs, the resulting PCE 0.95% is very low, from which it is hard to see the NP effect because of similarly low PCE 0.74% of P3HT/PCBM OPVs without CdS NP [40]. Very recently, a near-IR absorption PbS NP hybrid P3HT/PCBM system has been reported, although it is a photodiode study irrelevant to OPV [41]. Similarly, long wavelength (~700 nm) absorption CdTe NP hybrid P3HT/PCBM system has shown no photovoltaic characteristic but photoconductive gain for photodetectors [42].

2. Experiments

2.1. Instrumentation and measurement

2.1.1. Transmission electron microscopy (TEM) measurements

P3HT:PCBM of 1:0.8 weight ratio or various weight ratios of NP-containing P3HT:PCBM samples were dissolved in o-dichlorobenzene. The solution was then added dropwise onto the carbon films on copper grid (200 mesh). Each sample was then heated at 60 °C for 2 h at ambient environment and then transferred to a vacuum oven to remove the residue organic solvent for 16 h. The measurements were performed using a JEOL JEM-2010 transmission electron microscope (200 kV accelerating voltage and LaB6 filament).

2.1.2. Atomic force microscopy (AFM) measurements

The substrates (ITO glass) were first coated with PEDOT:PSS and then P3HT:PCBM:NP hybrid. Each sample was heated at 150 °C for 10 min for the thermal annealing treatment. The measurements were carried out with a multimode atomic force microscope (Digital Instruments, Nanoscope III) using tapping mode with a silicon tip.

2.1.3. Scanning electron microscopy (SEM) measurements

The substrates (Si wafer) were coated with P3HT:PCBM:NP thin films and heated at 150 °C for 10 min for the thermal annealing treatment. The sample for cross-sections examination was prepared on ITO-coated glass. The measurements were performed using a JEOL JSM-6700 field-emission scanning electron microscope, having resolution of 1.0 nm (15 kV) or 2.2 nm (1 kV), accelerating voltage in the range of 0.5–30 kV, and the magnifying scale of 25–650,000.

2.1.4. Optical and fluorescence microscopy measurements

The substrates (quartz plates) were spin-coated with P3HT:PCBM or P3HT:PCBM:NP thin films and heated at 150 °C for 10 min for the thermal annealing treatment. The measurements were conducted using an Olympus BX51 microscope with an objective lens of Olympus MPlanFL N (100X/NA 0.9). For the fluorescence images, the excitation wavelength was set at 510–550 nm and the detecting wavelength was greater than 590 nm. We used CoolSNAP HQ2 air cooled CCD as the detector.

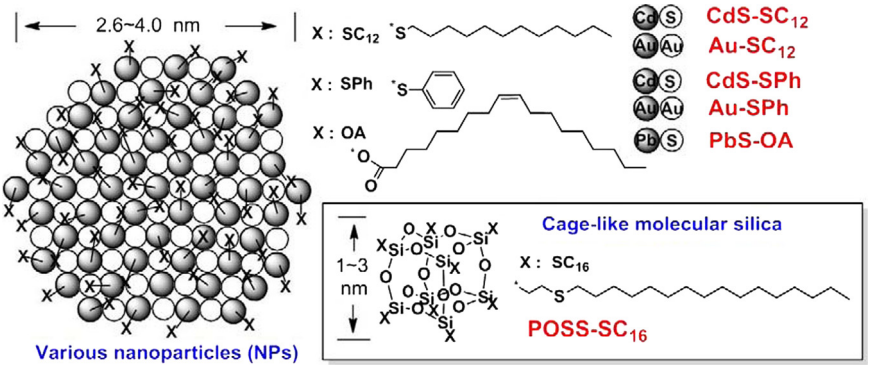

Scheme 1. Schematic illustration of the composition and size of NPs and the chemical structure of their surface capping agent (x).

2.1.5. Low-energy Photoelectron Spectrometer (AC-2) measurements

The sample of P3HT or various NPs powder was put on the metal disc for the measurements. The measurements were performed using a Riken-Keiki AC-2 photoelectron spectrophotometer. The Model AC-2 is an instrument for Photoelectron Spectroscopy at atmospheric pressure that is an open counter equipped with a UV source.

2.1.6. Powder X-ray diffraction (XRD) measurements

The substrates (ITO glass) were first coated with PEDOT:PSS and then P3HT:PCBM:NP hybrid. Each sample was heated at 150 °C for 10 min for the thermal annealing treatment. The measurements were carried out by using the Philips X'Pert diffractometer equipped with an X'Celerator detector. The radiation used was a monochromatic Cu Kα beam of wavelength $\lambda = 0.154$ nm.

2.1.7. UV–visible absorption spectrophotometer (UV–vis) measurements

The substrates (ITO glass) were first coated with PEDOT:PSS and then P3HT:PCBM:NP hybrid. Each sample was heated at 150 °C for 10 min for the thermal annealing treatment. For NP spectra acquired from solution, chloroform was used as the common solvent, except DMF was used for CdS-SPh. Except for PbS-OA, the UV–vis measurements were performed using a Hewlett-Packard 8453 spectrophotometer. A PerkinElmer Lambda 900 spectrophotometer was used for the NIR absorption measurements.

2.1.8. Fluorescence spectrophotometer (PL)

The substrates (ITO glass) were first coated with PEDOT:PSS and then P3HT, P3HT/PCBM, or P3HT:PCBM:NP hybrid. Each sample was heated at 150 °C for 10 min for the thermal annealing treatment. The PL measurements were performed using a Hitachi F-4500 fluorescence spectrophotometer.

2.1.9. Time-of-flight (TOF) method for measuring charge mobility

The TOF sample was prepared by spin-coating of ternary hybrid solution on O_2 plasma pre-treated ITO glass, similar to those in OPV fabrication. Subsequently, the hybrid thin film (~1 μm thickness) was deposited with Ag contact electrode (~100 nm) in a vacuum chamber. The equipment setup and experimental detail of TOF measurement can be found in our previous report [43–44].

2.2. Materials preparation

2.2.1. General materials

All solvents and chemicals were of reagent grade and used as received. P3HT, PCBM and poly(3,4-ethylenedioxythiophene):poly (styrenesulfonate) (PEDOT:PSS) used in OPV fabrication were purchased from Rieke Metals, Nano-C, and H. C. Starck (Baytron AI 4083), respectively. Two kinds of Au NPs, Au-SC_{12} and Au-SPh, bearing a surface capping thiol (dodecanethiol and thiophenol, respectively) were prepared according to the two-phase reduction method reported by Brust et al. [45]. Near-infrared absorbing PbS NPs (PbS-OA) bearing a surface capping oleic acid were prepared successfully based on a solution phase method reported by Hines et al. previously [46]. The preparation of dodecanethiol surface capping cadmium sulfide NPs (CdS-SC_{12}) was best achieved with a quaternary water-in-oil microemulsion approach [47]. On the other hand, we used a sol process in preparing thiophenol surface capping cadmium sulfide NPs (CdS-SPh) [48]. NPs CdS-SPh prepared from this process (acetonitrile is used as a co-solvent to dissolve cadmium acetate and thiophenol) have a better solubility in polar organic solvents. Octakishexadecanthiolethyl attached polyhedral oligomeric silsesquioxane (POSS-SC_{16}) is synthesized with 80% isolated yields from octavinyl oligomeric silsesquioxane (OvPOSS), which is previously known and synthesized via hydrolysis and condensation of vinyltriethoxysilane in hydrochloric acid solution accordingly [49].

2.2.2. Synthesis of octakishexadecanthiolethyl polyhedral oligomeric silsesquioxane (POSS-SC_{16})

To a tetrahydrofuran solution (25 mL) were added octavinyl polyhedral oligomeric silsesquioxane (0.3 g, 0.47 mmol) and azobisisobutyronitrile (0.05 g, 0.30 mmol). The solution was stirred and heated to refluxing temperatures for 24 h. After cooling to room temperature, excess amount of acetonitrile was added resulting in white precipitates. The product was purified by recrystallization in tetrahydrofuran twice to afford analytically pure product (1.02 g, 0.38 mmol, 80% yield). ^{1}H NMR (400 MHz, $CDCl_3$): δ (ppm) 0.86 (t, $J = 6.8$ Hz, 24 H), 0.99 (t, $J = 8.0$ Hz, 16 H), 1.22–1.41 (m, 224 H), 2.50 (t, $J = 8.0$ Hz, 16 H), 2.58 (t, $J = 8.4$ Hz, 16 H). ^{29}Si NMR (100 MHz, $CDCl_3$): δ (ppm) −68.78. MALDI-TOF MS (m/z) calcd for [$C_{144}H_{296}OSi_8$+Ag]: 2807.99, Found: 2808.4. Anal. Calcd for $C_{144}H_{296}OSi_8$: C 64.03, H 11.05. Found: C 64.00, H 11.09.

2.3. Fabrication and measurement of OPV devices

Samples prepared for fabrication of BHJ OPVs are achieved by mixing 1:0.8 weight ratio of P3HT:PCBM together with various weight ratios of NPs in an organic solvent. For example, P3HT (25 mg) and PCBM (20 mg) together with CdS-SPh NPs (1.25 mg, 5 wt% of P3HT) were dissolved in o-dichlorobenzene (1.76 g). The solution mixture was stirred for 12 h at 50 °C in a glove box filled with nitrogen gas.

BHJ OPVs were fabricated by spin-coating a solution of P3HT/PCBM/NP hybrid in forming a thin film, which is sandwiched between a transparent anode and a metal cathode. The anode consisted of glass substrates pre-coated with indium tin oxide (ITO) (sheet resistance 12 Ω/sq), which was cleaned by ultrasonic treatment in detergent, deionized water, acetone and isopropyl alcohol sequentially. The ITO glass substrate was covered by a layer (~30 nm) of spin-coated PEDOT:PSS solution (after passing through a 0.45 μm filter). After baking at 140 °C for 10 min, the PEDOT:PSS-coated ITO glass substrates were transferred to a nitrogen-filled glove box (O_2 and $H_2O < 0.1$ p.p.m.). The cathode consisted of Ca (~20 nm) top-capped with Al (~100 nm), and was thermally deposited under high vacuum conditions (8×10^{-6} Torr). The device active area is 0.04 cm^2, which was defined by the shadow mask adopted in the deposition of cathode electrode. The active layer (P3HT:PCBM:NP) was obtained by spin-coating the hybrid solution blends (after passing through a 0.22 μm filter) at 700 r.p.m. for 30 s and the thickness of film was 210–230 nm as measured with a surface profiler (Veeco Dektak 150). The spin-coated active layer was allowed to dry under cover of a glass Petri dish. Before cathode deposition, the films were thermally annealed at 150 °C for 10 min.

The current density–voltage (J–V) characteristics of the BHJ OPVs were measured under air atmosphere using a Keithley 2400 source measurement unit. The photocurrent was measured under AM 1.5 G 100 mW/cm^2 illumination from a class A solar simulator (Oriel 300 W). The light intensity was determined using a Si photodiode (PVM 172; area = 3.981 cm^2) which was calibrated by the National Renewable Energy Laboratory (NREL). For monochromatic incident photon-to-current efficiency (IPCE) or external quantum efficiency (EQE), an AM 1.5 G solar simulator was used to generate the bias light. A monochromator (Newport Model 74100), which was a National Institute of Standards and Technology calibrated photodiode and chopped at 250 Hz, was used to select the wavelengths between 350 and 800 nm for illuminating the device. The photocurrent from the polymer solar cell devices were measured through the lock-in amplifier (Signal Recovery 7265), which were in turn referenced to the chopper frequency. All electrical measurements were carried out under air atmosphere.

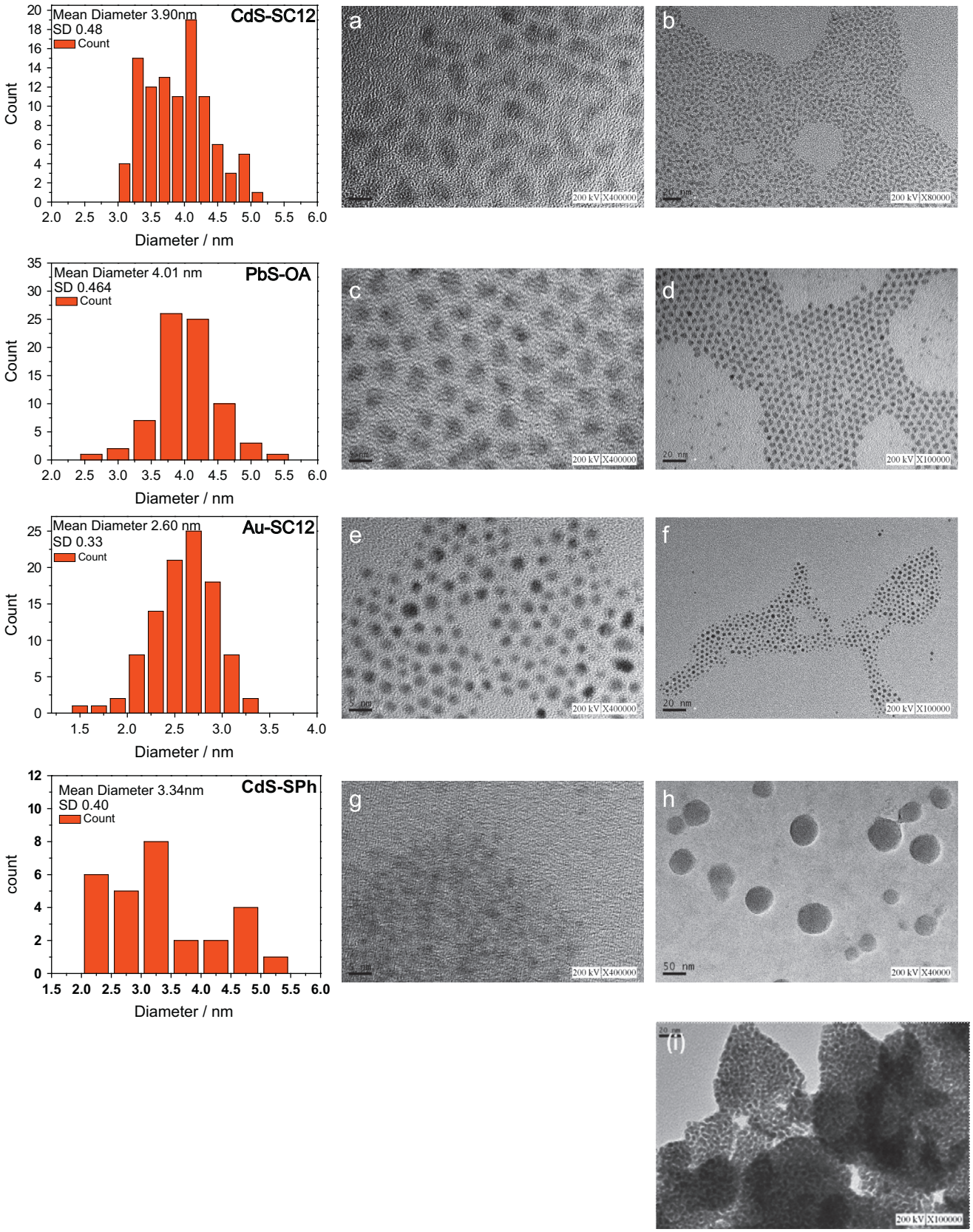

Fig. 1. TEM images of CdS-SC_{12} (a and b), PbS-OA (c and d), Au-SC_{12} (e and f), CdS-SPh(g and h), and (i). The scale bars are 5 nm for (a), (c), (e), and (g); 20 nm for (b), (f), (h), and (i); and 50 nm for (d). The red bar graphs shown on the left are the statistical counting of nanoparticle size and the acquired average size. (For interpretation of the references to color in this figure legend, the reader is referred to the web version of this article.)

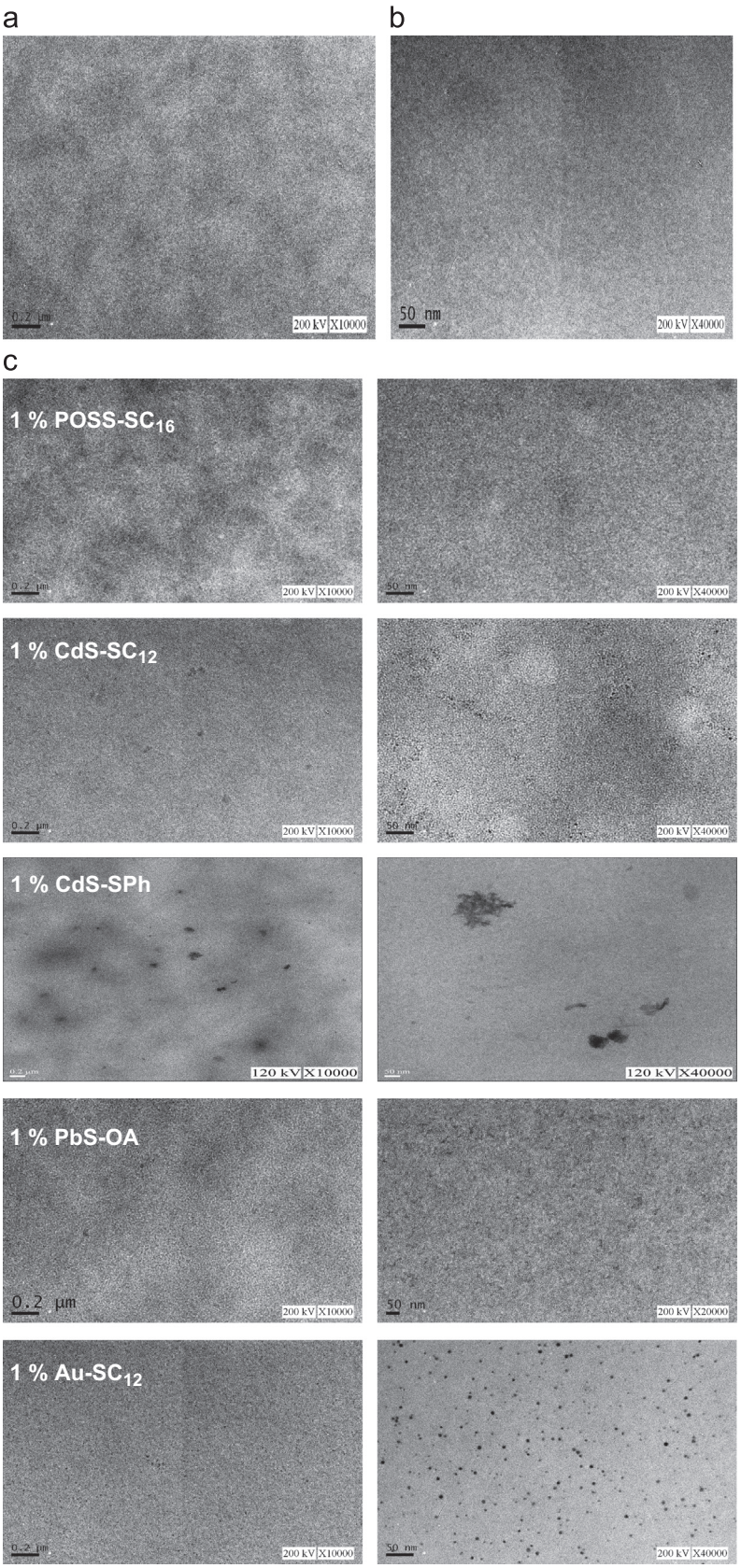

Fig. 2. TEM images of P3HT/PCBM thin films after thermal annealing at 60 °C (a and b), 1 wt% various nanoparticles doped P3HT/PCBM thin films after thermal annealing at 60 °C (c), and the respective 10 wt% NPs doped thin films (d). Note that the scale bar marked in the picture is equivalent to the length of 0.2 μm (× 10,000) and 50 nm (× 40,000) for the left and right figures in each set of images, respectively. However, four TEM images of CdS-SPh doped P3HT/PCBM thin film should be approximately enlarged 1.5 times in order to have the same scale as the other images shown in Fig. 2.

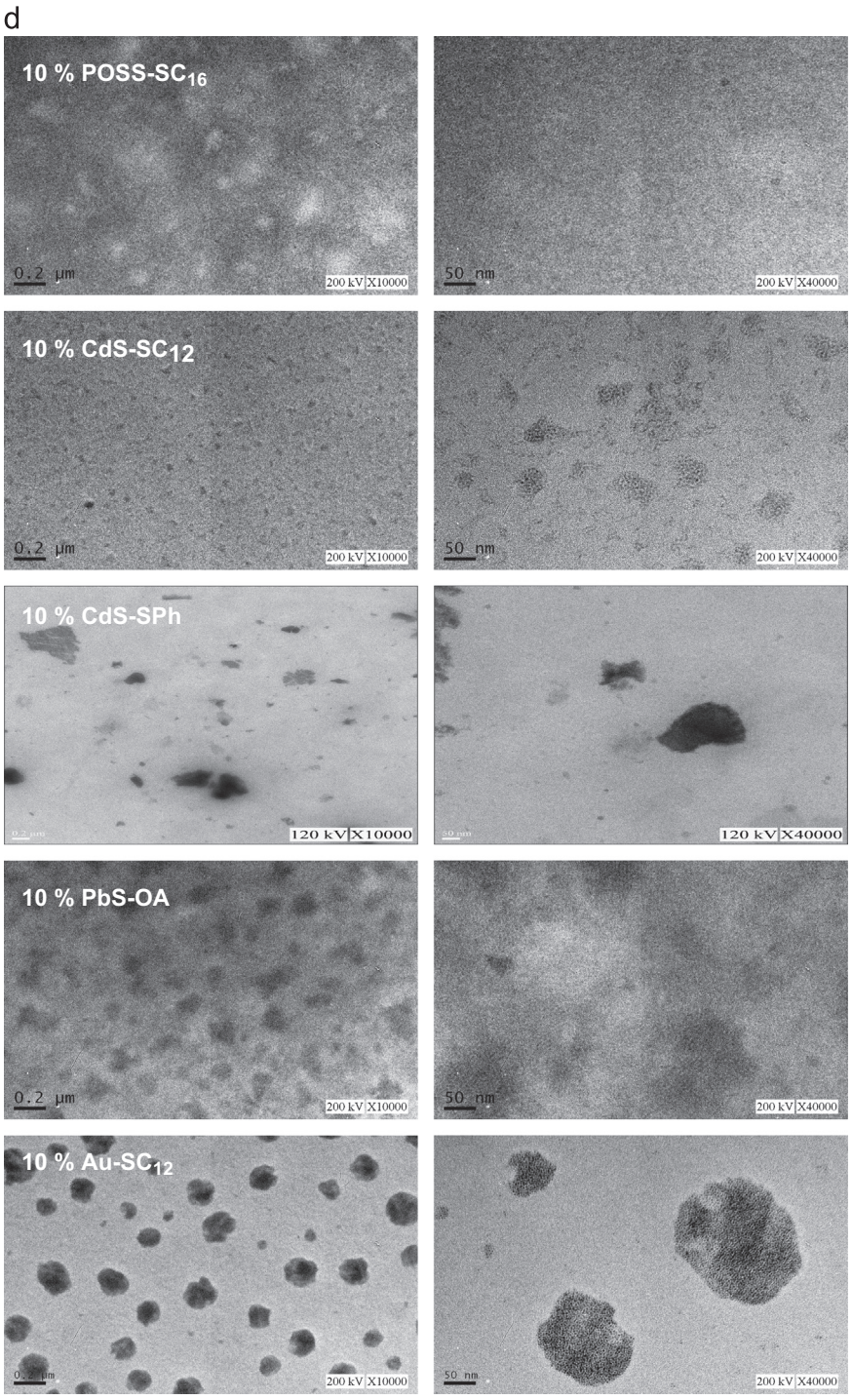

Fig. 2. Continued.

3. Results and discussions

3.1. Average size estimation of organic capped NPs

Except POSS-SC16, the particle size of all prepared NPs was estimated from their tunneling electron microscopy (TEM) images (Fig. 1). We estimated the statistical average size of these NPs from their respective TEM images. They are 3.9, 3.3, 4.0, and 2.6 nm for CdS-SC_{12}, CdS-SPh, PbS-OA, and Au-SC_{12}, respectively. We did not estimate the average particle size of Au-SPh due to its serious agglomeration and/or aggregation, which prohibits the sample preparation from solution as well as its fabrication process for BHJ OPVs. Similar agglomeration and/or aggregation but to a lighter extent are also discernible in the TEM images of CdS-SPh (Fig. 1(c) and (d)). In light of the surface capping agent being the same aromatic thiophenol for both CdS-SPh and Au-SPh, the superior power of the aliphatic hydrocarbon in the dispersion of NPs is quite evident for CdS-SC_{12}, PbS-OA, or Au-SC_{12}. The agglomeration and/or aggregation tendency of CdS-SPh cause a broader and less uniformed size distribution, which reduces the accuracy of size estimation based on TEM images.

Unlike other NPs in the present study, POSS-SC_{16} is a molecular silica compound having a cage-like spherical geometry. Due to the poor contrast in TEM images, its size estimation is best based on

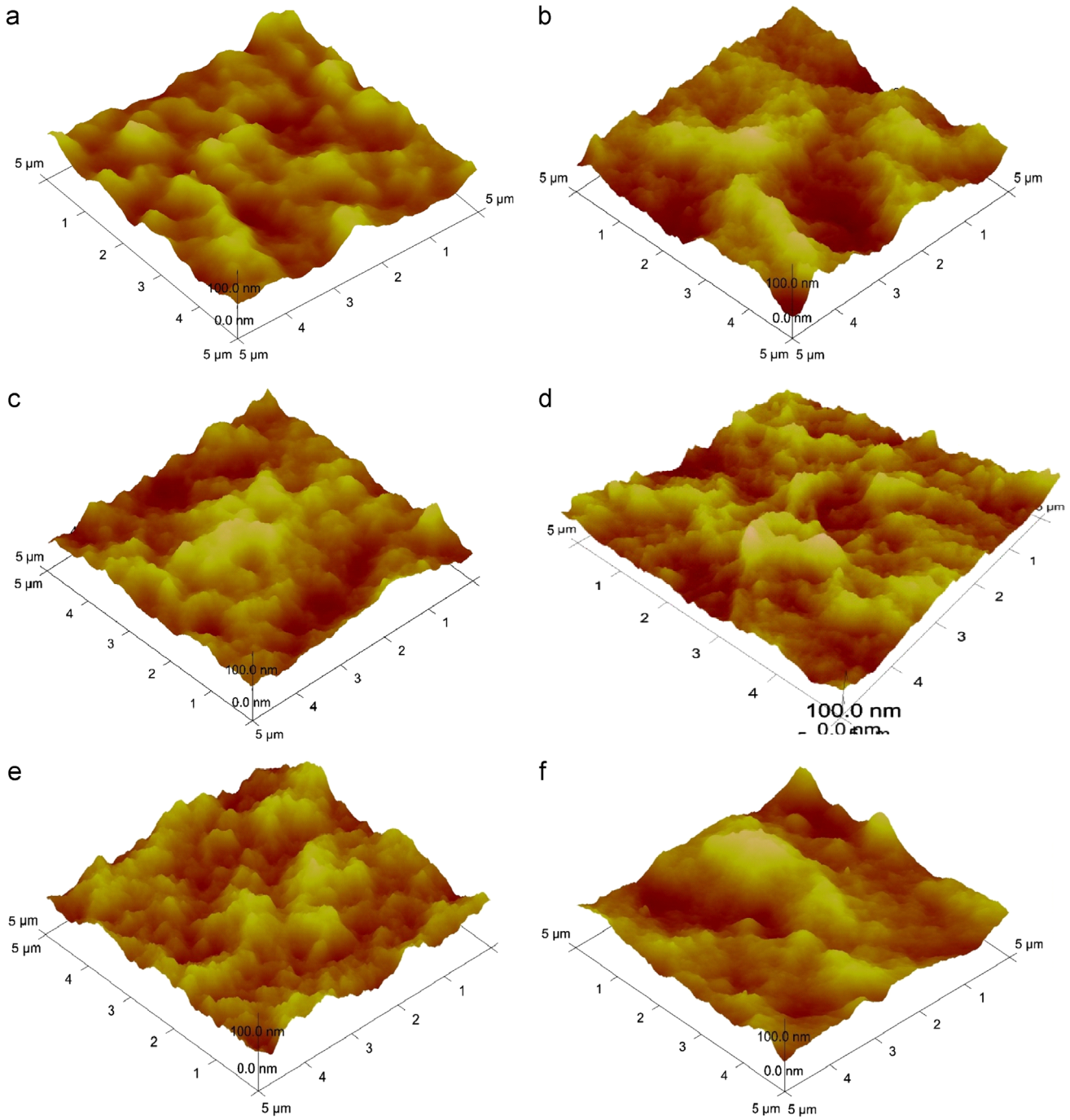

Fig. 3. AFM topography images ($5 \times 5\ \mu m^2$) of P3HT/PCBM thin films with thermal annealing (a), NP-doped (10 wt%) P3HT/PCBM thin film with thermal annealing: POSS-SC_{16} (b), CdS-SC_{12} (c), CdS-SPh (d), PbS-OA (e), and Au-SC_{12} (f).

the theoretical model or other experimental measurement. Its rigid core (Si_8O_{12}) has a diameter about 0.5 nm and becomes larger (1.5 nm) when the eight vertex groups are included [50–53]. Depending on the extension of these saturated hydrocarbon chains, eight hexadecanthiolethyl vertex groups of POSS-SC_{16} readily enlarge the particle size over 3 nm.

3.2. TEM and AFM surface images of P3HT/PCBM blended thin films doped with various NPs

It is conceivable that the agglomeration and/or aggregation of NP dopant influence the active layer morphology of P3HT/PCBM OPVs, which is in turn decisive for exciton diffusion, charge separation, charge transport, charge recombination, and eventually PCE of the device. Microscopic method like TEM or atomic force microscopy (AFM) is one of the commonly used techniques in probing surface morphology. Except POSS-SC_{16}, all NPs studied herein have heavy atom content (and hence higher electron density) compared with P3HT or PCBM resulting in high contrast features in TEM images. Therefore, TEM is particularly useful in showing agglomeration and/or aggregation characteristics of these NPs and their hybrid usage in P3HT/PCBM thin film. As a control image, Fig. 2(a) and (b) shows the thermally annealed thin film sample of P3HT/PCBM. Probably due to the moderate thermal annealing temperature (in order to avoid the detachment of carbon film on TEM copper grid) or the low resolution of the TEM, our TEM images do not show fibrillar P3HT crystallite, which is usually the distinctive feature of the higher temperature (120–150 °C) annealed P3HT/PCBM thin film [23]. However, our

moderate annealing temperatures (60 °C) already induce agglomeration and/or aggregation of NP dopant, as shown in Fig. 2(c) and (d) for 1 and 10 wt% of NP dopant P3HT/PCBM thin film, respectively. In terms of the size or darkness of features in TEM images, all NPs show agglomeration and/or aggregation, more or less, and CdS-SPh and Au-SC_{12} NPs are the two most prominent ones. Interestingly, there are a number of bright spots in the TEM images of POSS-SC_{16} doped (1 wt %) P3HT/PCBM. In the TEM images of 10 wt% POSS-SC_{16} doped P3HT/PCBM thin film, such bright spots or lumps (with average size of less than 100 nm) are much more in number. We presume that such bright feature in the TEM image is due to the agglomeration and/or aggregation of POSS-SC_{16} NP, the chemical structure of which does not contain heavy atom or any π-electron.

On the other hand, we have also recorded the AFM surface images on the thermally annealed P3HT/PCBM thin film and its NPs hybrid (10 wt%) thin film. With annealing temperature around 150 °C, the acquired AFM image of P3HT/PCBM (Fig. 3(a)) shows great resemblance to those reported in literature [21]. Based on the TEM shown in Fig. 2d, the size of the agglomeration and/or aggregation of the NPs is in the submicrons region and is not easy to be differentiated in the AFM image with a scanning area of $5 \times 5\ \mu m^2$ (Fig. 3). However, comparing with Fig. 3(a), the lumpy feature in AFM images (Fig. 3(b–f)) of NP hybrid P3HT/PCBM thin film tends to be larger in size. Although the content of these lumps awaits further analysis, such AFM images may indicate the agglomerated and/or aggregated NPs contained inside.

3.3. *Scanning electron, optical, and fluorescence microscopic methods in observation of P3HT/PCBM/CdS-SPh blends with various composition ratios*

Greater than μm size agglomeration and/or aggregation of NP dopant are most evident from the scanning electron microscopy (SEM) surface images of P3HT/PCBM/CdS-SPh blends with various compositions (Fig. 4). Without CdS-SPh NP dopant, thermally annealed P3HT/PCBM thin film shows SEM image (with under-

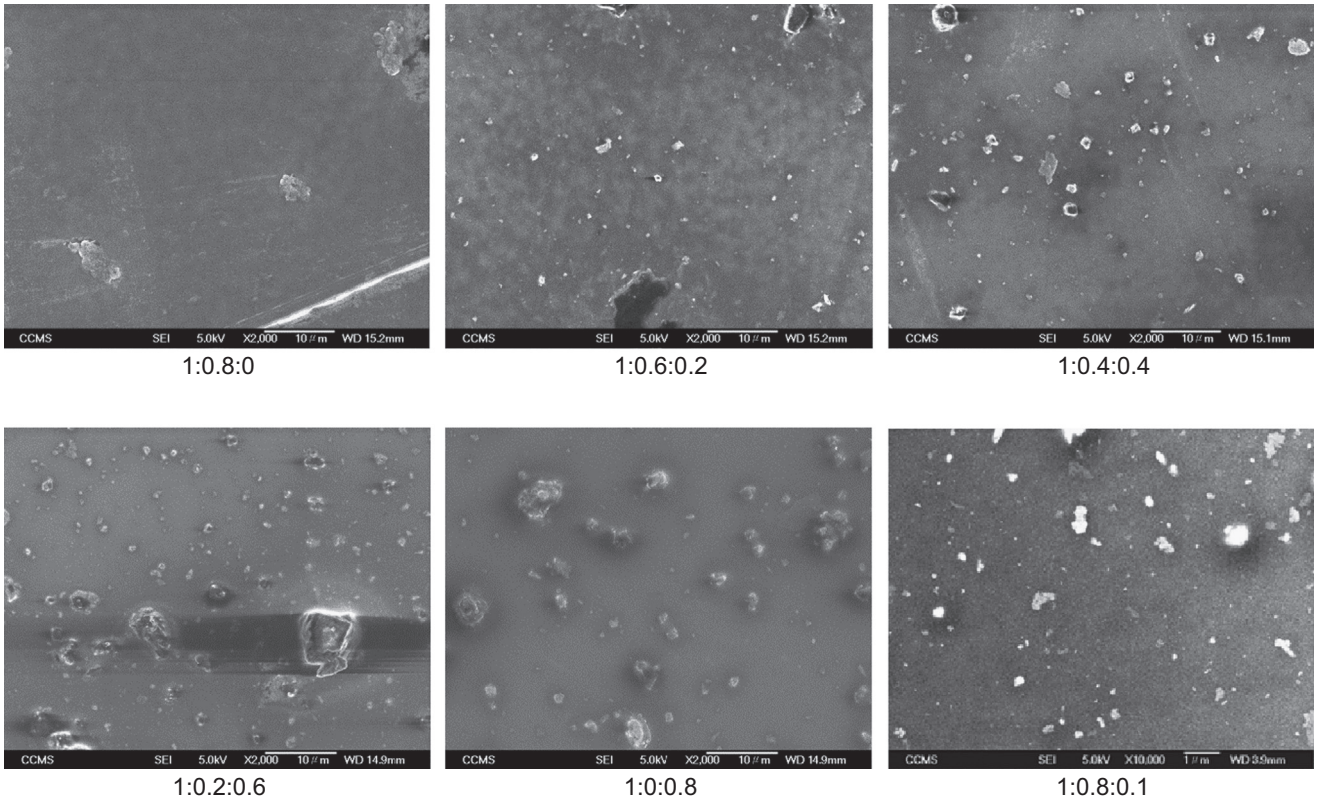

Fig. 4. SEM surface images (ca. $50 \times 40\ \mu m^2$ and $\times 2000$ magnifying scale) of P3HT/PCBM/CdS-SPh blends thin film with various composition ratios: 1:0.8:0, 1:0.6:0.2, 1:0.4:0.4, 1:0.2:0.6, and 1:0:0.8. Note that the bottom right SEM image is in a different magnifying scale ($\times 10{,}000$) and the thin film composition ratio is 1:0.8:0.1.

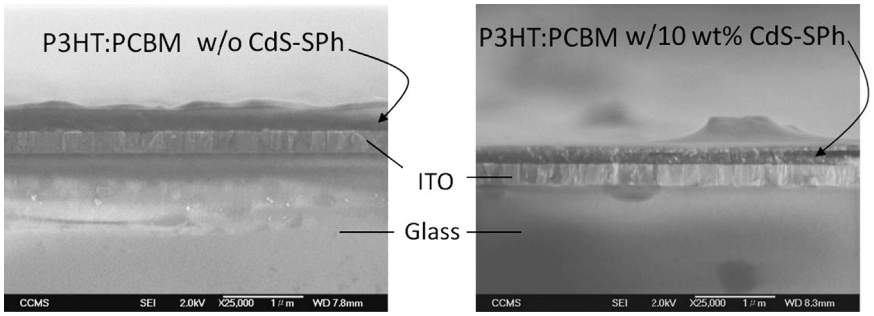

Fig. 5. SEM cross-section images of P3HT/PCBM thin films with (right figure) and without (left figure) 10 wt% CdS-SPh NP.

label of 1:0.8:0, and the composition ratio of P3HT/PCBM/CdS-SPh) having resemblance to that of P3DT (poly(3-dodecylthiophene))/PCBM [54], which exhibits feature of PCBM aggregation or crystal with a size of less than 10 μm, consistent to what we have reported earlier [55]. When increasing ratio of CdS-SPh NP component at the same time decreasing ratio of PCBM in proportion, somewhat different features emerge in SEM photos and they are much more in quantity (see photos with under-label of composition ratios 1:0.6:0.2, 1:0.4:0.4, 1:0.2:0.6, and 1:0:0.8, in Fig. 4). Based on the energy dispersive spectrometer (EDS) elemental composition analysis, these somewhat different but much more in quantity SEM features have been detected with increasing cadmium content along with increasing CdS-SPh NP composition ratio in the thin film. SEM and EDS together infer that these SEM features contain agglomeration and/or aggregation of CdS-SPh NP.

As shown in SEM images (Fig. 4), the agglomeration and/or aggregation of CdS-SPh NP is somewhat different from that of PCBM. It is more sharp-edged and it is more high-rise in vertical direction. Such different features of sharp-edged and high-rise are more revealing in the SEM cross section view of P3HT/PCBM/NP thin films (see Fig. 5).

With an even larger size of ~1 mm under the optical microscope, thermally annealed thin film of P3HT/PCBM blends shows distributed dark spots with a size of submicrons up to a couple of μm (Fig. 6(a)). This kind of optical micrograph has been reported before by other research groups and it was attributed to the microcrystals of PCBM [56–58]. Under the fluorescence microscope, the same dark spots in optical micrograph all lit up in the dark background (Fig. 6(b)). In fact, in the micrograph with larger magnifying scale (not shown here), each PCBM microcrystal is surrounded by a bright region, a PCBM-depleted region composed by almost pure P3HT according to the inference in literature [59]. Unlike the perfect match between bright and dark spots in Fig. 4 (a) and (b), when 10 wt% of CdS-SPh NP dopant is included in P3HT/PCBM blends, a few "mismatched spots" (brightness and darkness are not proportional in size) emerge and they are marked by gray or white arrows in Fig. 6(c) and (d). Such "mismatched spots" become much more in number when the amount of CdS-SPh NP increases to 20 wt% (see Fig. 6(e) and (f)). Clearly, the agglomerated and/or aggregated CdS-SPh NPs play a role in these "mismatched spots" observed by optical and fluorescence microscopes, which are consistent with that observed in SEM images.

3.4. Band-gap energy determination of various NPs and their light absorbance compared with P3HT/PCBM

We used onset absorption wavelength acquired from solution absorption spectra of NPs for the estimation of optical band-gap energy. One special case requires noting here for the metallic NP, i.e., Au-SC_{12}. The energy estimated for Au-SC_{12} is in fact the surface

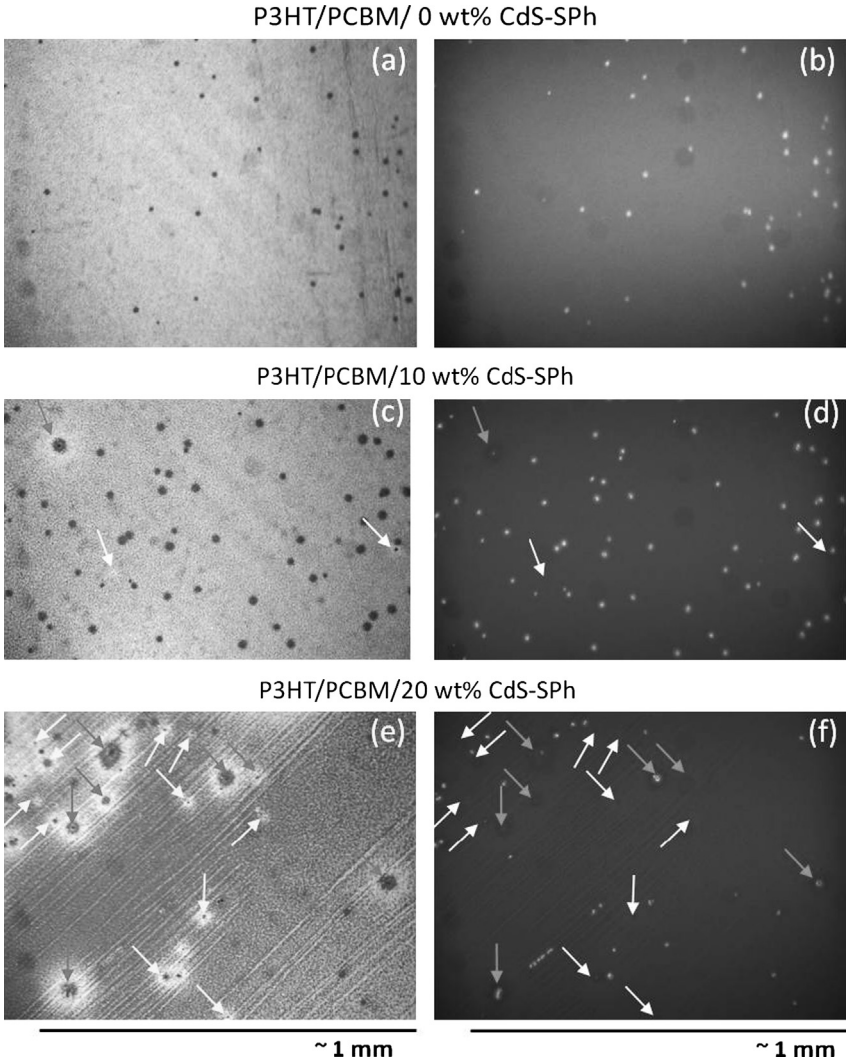

Fig. 6. Images of P3HT/PCBM or P3HT/PCBM/CdS-SPh thin films under optical (left figures) and fluorescence (right figures) microscopes.

plasmon resonance energy, which is different from the optical band-gap energy determined for the semiconducting or insulating NPs. As shown in Fig. 7, POSS-SC_{16} is transparent to the visible light and has absorption wavelength less than 320 nm. CdS-SC_{12} is yellow due to the absorption λ_{max} ~400 nm (λ_{onset} ~470 nm). Because of its smaller particle size, CdS-SPh is virtually colorless showing very faint yellow color in diluted solution having λ_{max} ~360 nm (λ_{onset} ~400 nm). Both PbS-OA and Au-SC_{12} NPs appear dark in solution due to the near panchromatic absorption centered at the near-IR (λ_{max} ~1100 nm and λ_{onset} ~1191 nm) and visible regions (λ_{max} ~520 nm and λ_{onset} ~710 nm), respectively. The onset absorption of P3HT thin film sample was also determined for reference and it is around 645 nm (1.92 eV).

Although there is visible light or near-IR absorption, the absorbance of CdS-SC_{12}, CdS-SPh, PbS-OA and Au-SC_{12} NPs relative to that of P3HT/PCBM (1:0.8) is all too small to make any substantial contribution to light harvesting (Fig. 8). Even having NPs hybrid concentration as high as 40 wt%, light absorption of P3HT/PCBM is far more intense than that of NPs.

3.5. HOMO and LUMO energy levels determination of various NPs

We used a low-energy photoelectron spectrometer (Riken-Keiki AC-2) to determine the HOMO energy level or work function of the NP materials and P3HT as well as for comparison purpose. All AC-2 spectra of NPs and P3HT are summarized in Fig. 9.

Metallic and therefore conducting content of Au-SC_{12} has the smallest work function at 4.88 eV, which is not much different from 4.9–5.1 eV of bulk gold determined by an ultraviolet photoelectron spectrometer [60–62]. PbS-OA has the second shallowest HOMO energy level at 5.08 eV and this is rather close to 5.0 eV reported for tributylamine surface-capped PbS colloidal quantum dots recently [63]. Regardless of the difference in NP size or different surface capping agent (aromatic thiolphenol or aliphatic

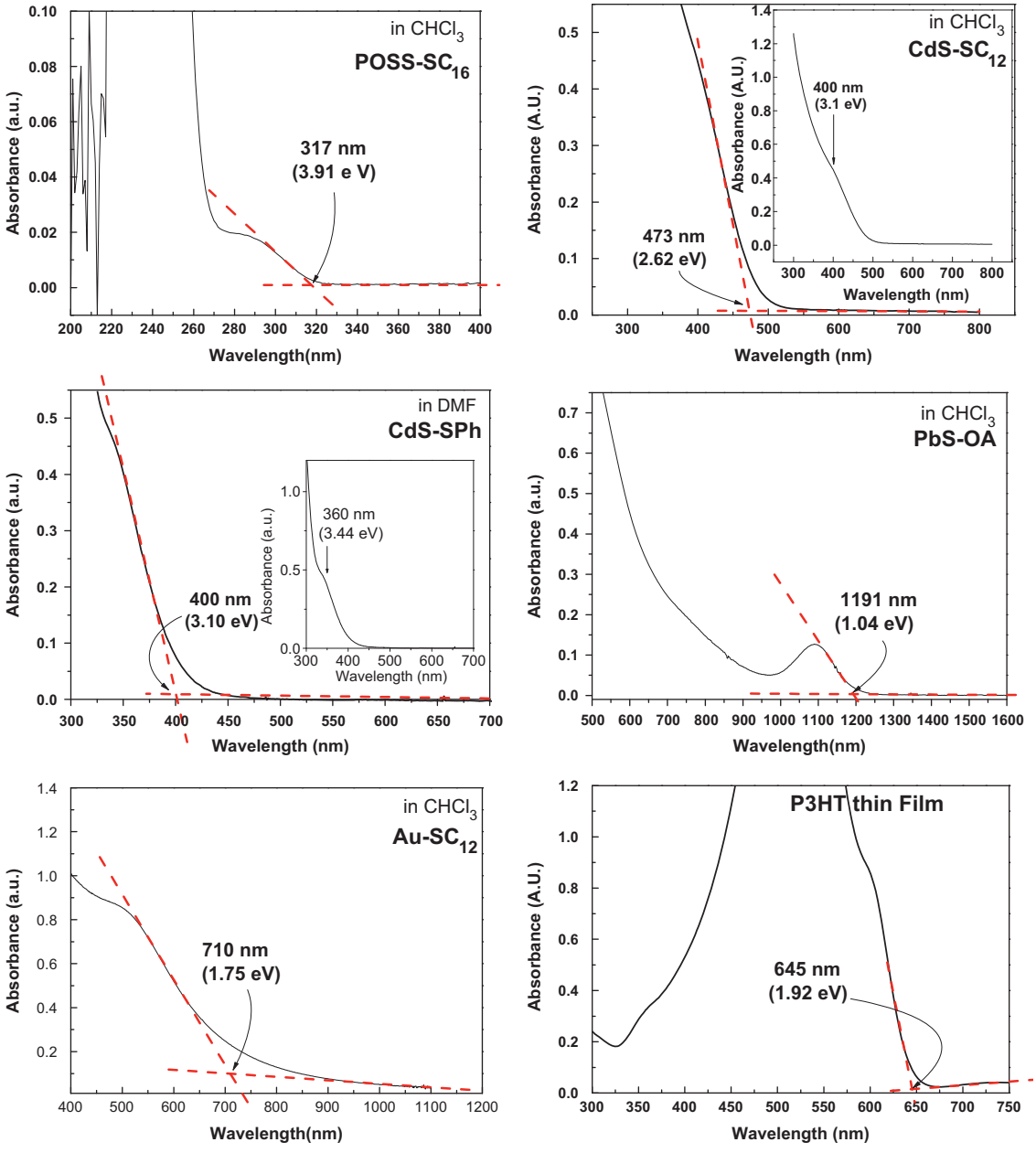

Fig. 7. UV–visible absorption spectra of various NPs in chloroform or DMF solution and P3HT thin film sample. Optical band-gap energy is estimated from the absorption onset wavelength.

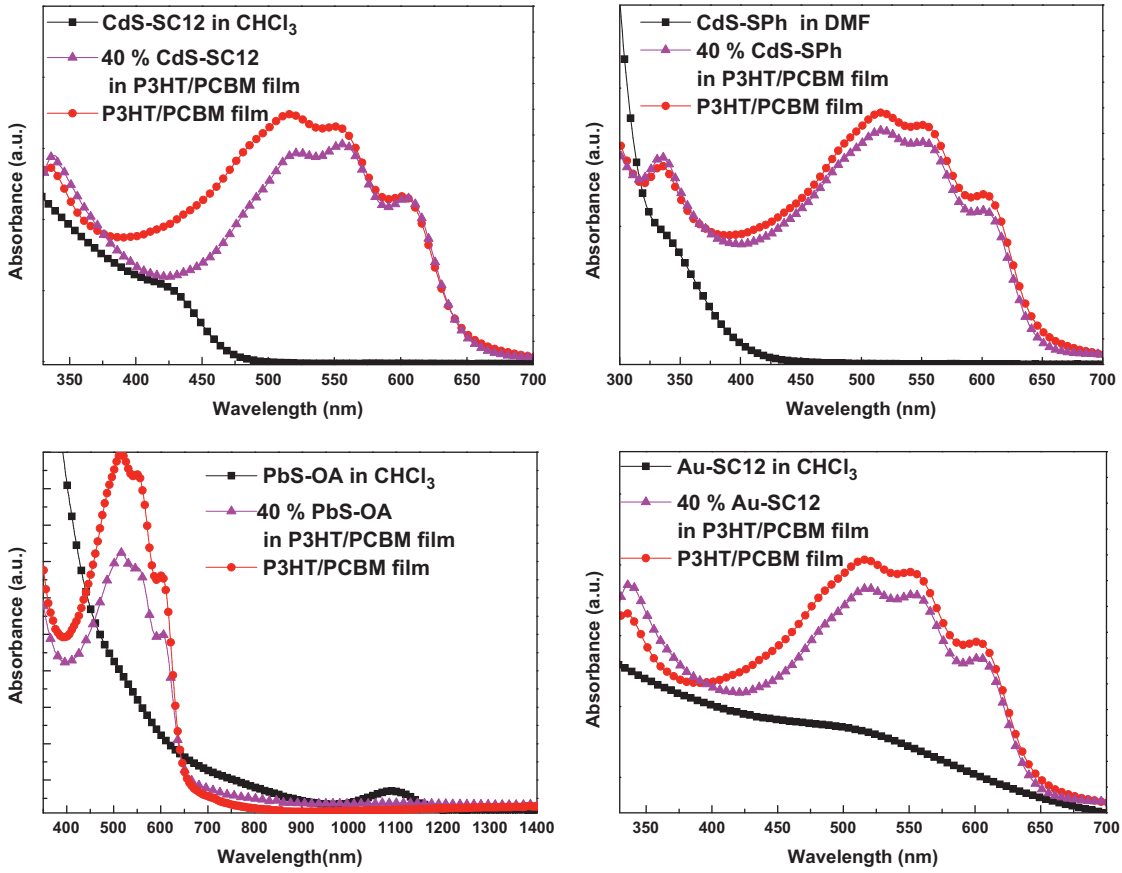

Fig. 8. UV–visible–NIR absorption spectra of P3HT/PCBM thin film and its NP-containing (40 wt%) thin films. Solution absorption spectra of NPs are included (adapted from Fig. 2) for identifying absorption wavelength. The absorbance of the thin film is normalized at 700 nm (for CdS-SC_{12}, Au-SC_{12}, and CdS-SPh) and 1400 nm (for PbS-OA).

hydrocarbonthiol), CdS-SC_{12} and CdS-SPh show very similar HOMO energy levels at 5.76–5.77 eV, which is significantly shallower than ~6.4 eV of the valance band of CdS bulk crystals [64]. Nevertheless, the difference of organic surface capping agent has little effect on the HOMO energy level of NPs, which is mainly determined by the material content inside of the NPs. All together, these NPs have a HOMO energy level or work function deeper than that of P3HT, which is as shallow as 4.75 eV (Fig. 9). Considering the HOMO energy level or work function of the NP hybrid P3HT/PCBM OPV system studied herein, P3HT is still the material responsible for hole transporting even in the presence of NPs.

Based on the HOMO energy level (or work function of Au NP) determined by AC-2 shown above in Fig. 10, the LUMO energy level of each NP (and P3HT as well) in the present study can be calculated with optical band-gap energy, which is estimated from the absorption onset wavelength shown in Fig. 7. HOMO and LUMO energy level alignment of various NPs, P3HT, and PCBM [65] ternary hybrid is depicted in Fig. 10.

Important information acquired from the energy level alignment is the feasibility of charge separation of P3HT exciton due to NPs. From the absorption spectra of various NPs and P3HT/PCBM, it is P3HT that dominates the light absorption and hence the generation of exciton in the BHJ OPVs. Based on the reported data in literature, exciton bonding energy for most organic materials is in the range of 0.4–0.5 eV [5]. For P3HT exciton, more than 0.3 eV is required to affect the exciton splitting and charge dissociation [66]. Accordingly, PbS-OA and maybe Au-SC_{12} are two kinds of NP enabling electron extraction from P3HT exciton because of appropriate energy level alignment or sufficient energy level offset. Electron extraction by POSS-SC_{16} is highly impossible due to the very high LUMO energy level. Electron extraction by CdS-SC_{12} or CdS-SPh is questionable because of the very close alignment of LUMO energy level or there is insufficient offset of LUMO energy levels.

3.6. *Spectroscopy probing the packing of P3HT in the presence of NPs*

As many literatures have reported (see Refs. [4,20,22] for examples), UV–visible absorption and X-ray diffraction (XRD) spectroscopy are potent tools in examining the packing or crystallite formation of the P3HT polymer chain. The appearance of vibronic absorption shoulder band ~550 and ~600 nm is the signature of the close packing of P3HT polymer chain in the condensed phase. On the other hand, the intensity of XRD signal at 2θ ~5.2° corresponding to side-to-side distance of the polymer chain (16–17 Å) reflects the domain size of P3HT packing or crystallite. As shown in Fig. 11, our UV–visible absorption and X-ray diffraction spectra both reveal that the NPs (10 wt% in P3HT/PCBM) have some influence on the packing or crystallite formation of P3HT polymer chain. Although such influence is just moderate, both spectra imply that CdS-SPh and POSS-SC_{16} are the most and the least influential NPs, respectively. In fact, such spectroscopic results are in accordance with the PCBM influence on that of P3HT polymer chain. Due to the aromatic and π-electron nature of PCBM, in the coexistent system of P3HT/PCBM, the aliphatic side chains of P3HT tend to repel PCBM but to attract P3HT itself. The different electronic nature of organic surface capping agent of CdS-SPh and POSS-SC_{16} makes the difference in repelling or attracting P3HT, although it is to a much smaller extent when compared with that of PCBM.

From the LUMO energy level of the materials and the spectroscopic data of P3HT, it seems that there is potential interaction between P3HT and some of the NPs studied herein. We used fluorescence spectroscopy to measure the quenching of P3HT

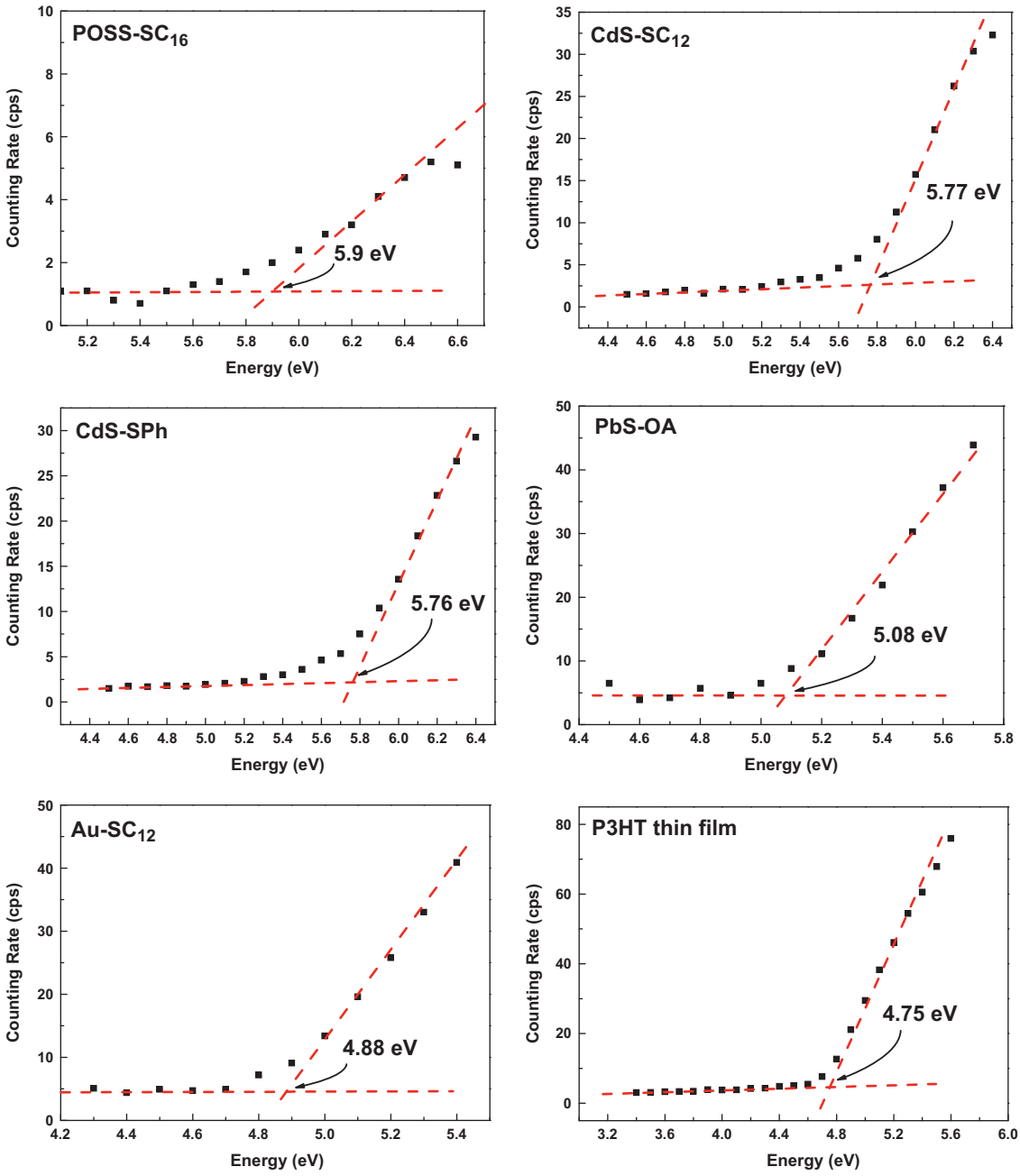

Fig. 9. Low-energy photoelectron spectra of NPs and P3HT thin film.

photoluminescence (PL) as a gauge for the electron transfer from the photo-excited P3HT to NPs. As a control reference, we first examined the variation of PL intensity of P3HT thin film with and without thermal annealing. As shown in the top left figure of Fig. 12, thermal annealing causes PL quenching of P3HT because of tighter or better packing of polymer chain, which confirms the inference from thermal annealing results shown by UV–visible absorption and X-ray diffraction spectroscopy. Second, as is being illustrated in many literatures, PL of P3HT is significantly quenched by blending with PCBM because of efficient electron transfer from the photo-excited P3HT to PCBM (as shown by red ball symbol lines in the rest of the figures in Fig. 12). Most interestingly, the PL intensity is somewhat enhancing, instead of diminishing, when NPs are doped (5 wt%) in P3HT/PCBM thin film (see green triangle symbol lines in Fig. 12).

Such PL enhancing results happen to all kinds of NPs studied herein, including PbS-OA, even though it has appropriate alignment and sufficient offset of LUMO energy levels. In addition to just alignment of LUMO energy level and its energy offset, a more comprehensive thinking about the electron transfer between P3HT and NPs is necessary. We think the long aliphatic-based organic surface capping agent, such as dodecanethiol of CdS-SC_{12} and Au-SC_{12}, hexadecanthiolethyl of POSS-SC_{16}, or oleic acid of PbS-OA, prevents NPs from proximate contact with P3HT. Moreover, the aliphatic hydrocarbon chain is insulating and essentially forms the charge or electron transfer barrier for NPs, which has been the case for surface capping TOPO (trioctylphosphineoxide) of CdSe NP [67–69]. Within the context, aromatic thiophenol of CdS-SPh NP seems fine for facilitating electron transfer from P3HT to CdS-SPh. Aromatic thiophenol is short and it is semiconducting due to the delocalized π-electron. As evidences have shown above, it even has some positive effects on promoting packing or crystallite formation of the P3HT polymer chain. However, LUMO energy alignment of CdS-SPh NP is not appropriate or its LUMO energy offset is not sufficient for the charge separation of

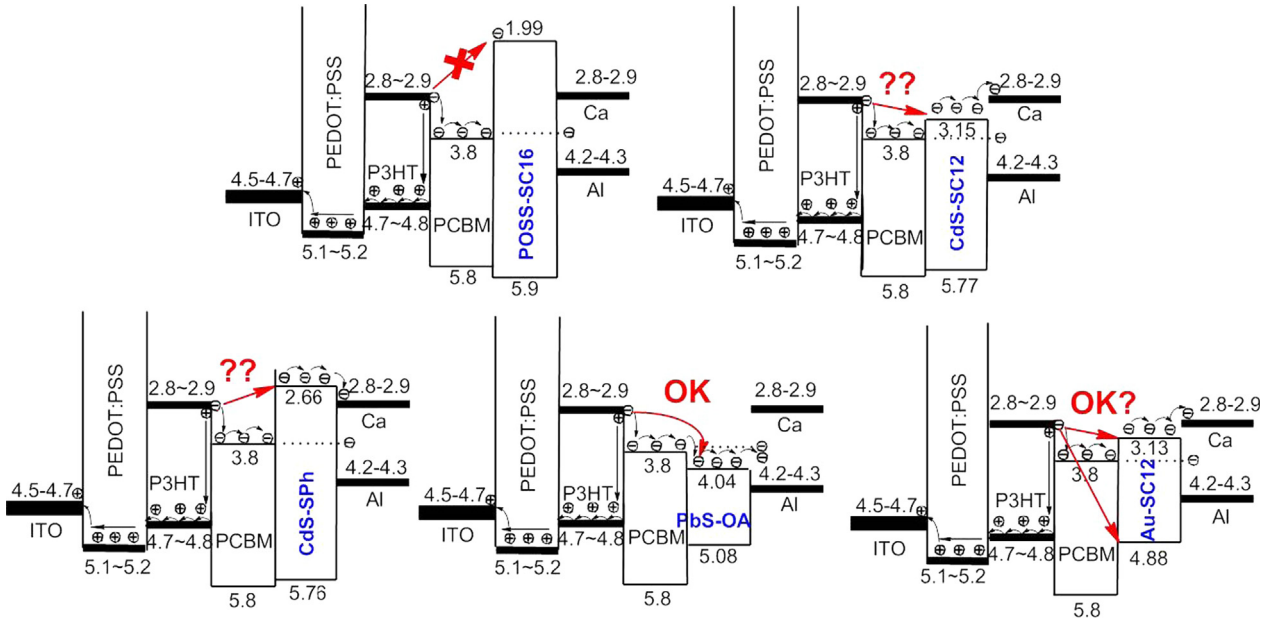

Fig. 10. HOMO and LUMO energy level alignment of various NPs, P3HT, and PCBM. For Au-SC_{12} NP, determined work function is the HOMO energy level and the corresponding LUMO energy level is derived from the energy of surface plasmon resonance. The estimation of charge separation of P3HT exciton due to NPs is marked in red color. (For interpretation of the references to colour in this figure legend, the reader is referred to the web version of this article.)

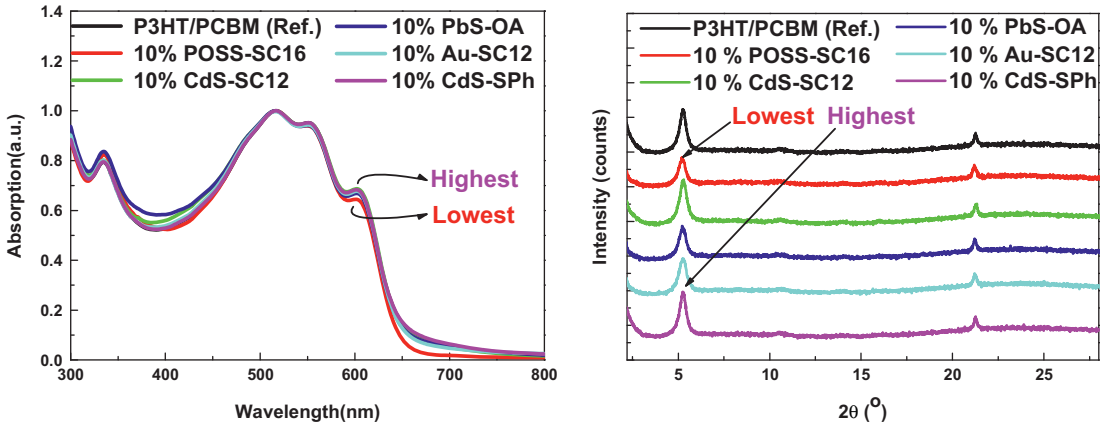

Fig. 11. *Left figure*: UV–visible absorption spectra of P3HT/PCBM and its NP-containing (10 wt%) thin films (on ITO/PEDOT:PSS-coated glass substrate) after thermal annealing. The intensity of all absorption spectra is normalized to the absorption peak of P3HT at 516 nm. *Right figure*: X-ray diffraction spectra of P3HT/PCBM and its NP-containing (10 wt%) thin films (on ITO/PEDOT:PSS coated glass substrate) after thermal annealing. The intensity of all diffraction spectra is normalized to the ITO diffraction signal at 2θ~21°.

P3HT exciton. Furthermore, agglomeration and/or aggregation are very serious (because of poor dispersion power of organic surface capping thiophenol) for CdS-SPh NP in P3HT/PCBM, which significantly reduces its physical contact and electronic interaction with P3HT. In the meantime, the presence of CdS-SPh NPs simply reduces the contact between P3HT polymer and PCBM molecule, which alleviates the PL quenching of P3HT as shown in Fig. 12. Therefore, we have a dilemma situation here for NPs hybrid P3HT/PCBM. We need an aliphatic-based organic surface capping agent in order to have a better dispersion of NPs in P3HT/PCBM blends. However, such an organic surface capping agent of NP is essentially insulating and blocking electron transfer from P3HT to NP, regardless of the LUMO energy level of NP.

3.7. Charge carrier mobility of CdS-SPh doped P3HT/PCBM blends

Regarding charge conductivity, CdS, the material content of CdS-SPh NP, is a well known *n*-type compound semiconductor [70], and it is the only NP that we successfully prepared with charge transporting organic surface capping agent (aromatic thiophenol). We have tried to replace the oleic acid of PbS-OA with SPh, resulting in an insoluble mass. A similar result happened to the conducting Au-SPh NP as mentioned earlier in the report. Fortunately, the poor solubility of CdS-SPh NP is just barely enough for moderate hybrid concentration (less than ~10 wt%) for the solution processing with P3HT and PCBM in OPV fabrication. In this regard, near-IR absorbing PbS-SPh (that we failed to acquire) and metallic Au-SPh NPs are simply not soluble enough for any device fabricated by solution process including sample preparation for the measurement of charge carrier mobility. In literature, dodecanthiol surface-capped CdS NP (i.e., CdS-SC_{12} in this study) has been shown for enhancing the hole mobility of poly(*N*-vinylcarbazyl) [64,71]. Although the electron transfer from P3HT to CdS-SPh NP is questionable or uncertain from the acquired experimental results so far, charge carrier mobility of CdS-SPh NP seems to be useful information to understand its impact on P3HT/PCBM BHJ OPVs. Charge carrier mobility of P3HT/PCBM with or without CdS-SPh NP dopant (10 wt%) was determined by time-of-flight (TOF) transient photocurrent measurement. CdS-SPh NP was found promoting charge carrier

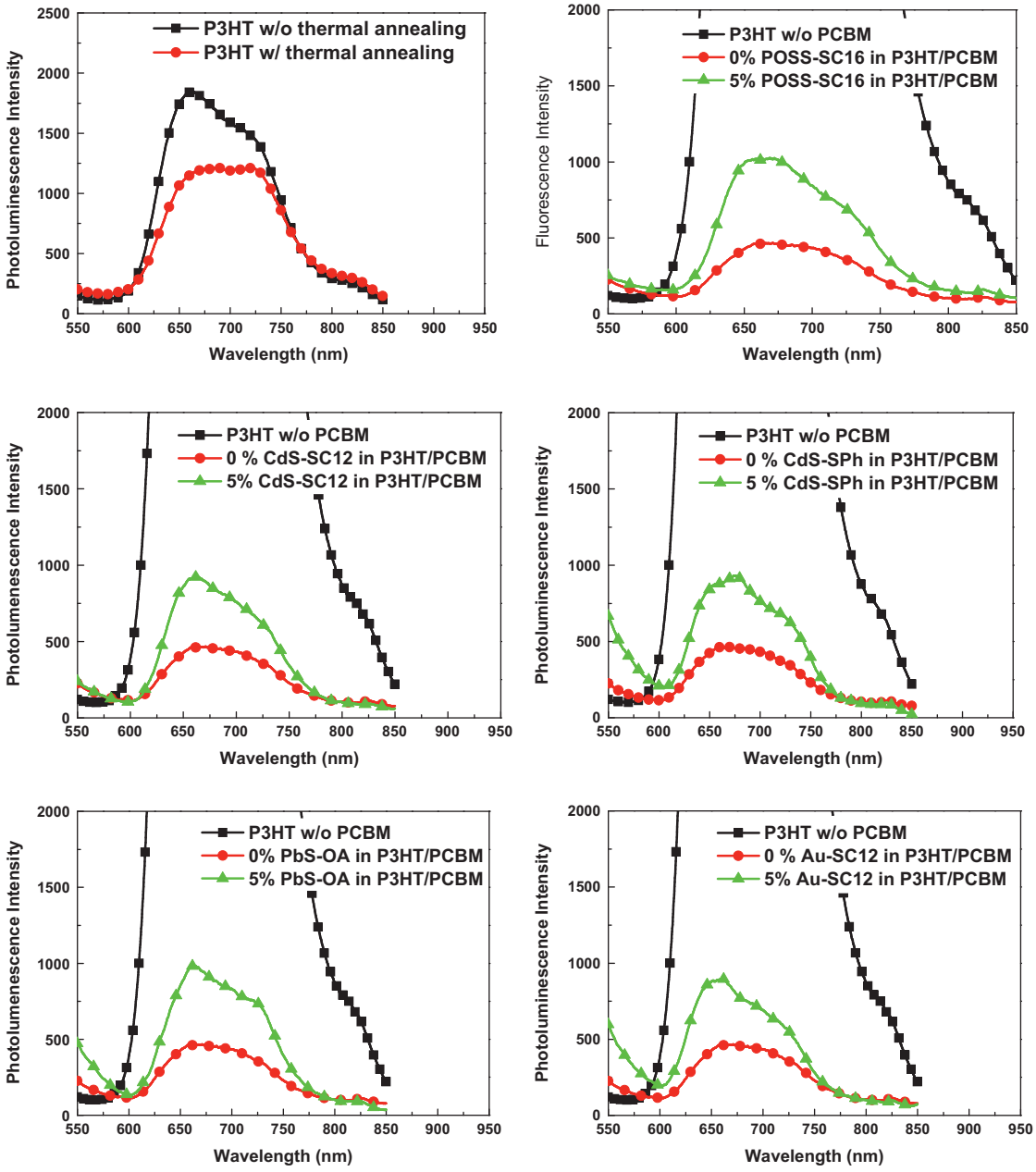

Fig. 12. *Top left figure*: photoluminescence spectra of P3HT thin film with and without thermal annealing treatment. *The other five figures*: P3HT thin film (black square symbol lines), P3HT/PCBM thin film (red ball symbol lines), P3HT/PCBM thin film containing various 5 wt% nanoparticles (green triangle symbol lines) all with thermal annealing treatment. (For interpretation of the references to colour in this figure legend, the reader is referred to the web version of this article.)

mobility, both hole and electron, of P3HT/PCBM blends (Fig. 13). Such results are quite inspiring for improving performance of BHJ OPVs. However, this is not necessarily the case (see the next section for details). In the NP hybrid BHJ P3HT/PCBM OPVs, P3HT dominates the exciton generation and the subsequent hole transportation, whereas PCBM is mainly responsible for the electron transportation. Unlike the charge generation in all places in the TOF charge mobility measurement, in the OPV system tested here, CdS-SPh NP is not the major charge (electron) carrier and receiving electron from P3HT does not seem feasible as demonstrated in the present study.

3.8. Bulk heterojunction P3HT/PCBM OPVs containing various NP dopants

Two types of NPs-containing P3HT/PCBM OPVs were fabricated by solution process. First, the composition weight ratio of P3HT and PCBM is set at a constant of 1–0.8. We blend in POSS-SC_{16}, CdS-SC_{12}, CdS-SPh, PbS-OA, and Au-SC_{12}, five NPs as dopant hybrid (3 or 5 wt%) in BHJ P3HT/PCBM OPVs. Corresponding current density characteristics of 3 wt% NP-containing OPV, either under simulated sun illumination or in the dark, are displayed in Fig. 14(a) and (b), respectively. Table 1 summarizes the data of short circuit current (J_{SC}), open circuit voltage (V_{OC}), fill factor (FF), and PCE of these devices, including P3HT/PCBM without any NP dopant hybrid as the control OPV.

From the data, PCE of NP-containing devices is all deteriorated ($<4\%$) when compared with the control of P3HT/PCBM, the PCE of which is 4.01%; the higher the NP concentration, the worse the performance (PCE) of the device. A similar trend happens to V_{OC} and FF of these devices. Differently, except POSS-SC_{16} one, NP-containing devices show more or less enhanced J_{SC}, when compared with the control P3HT/PCBM. This is consistent with the

insulating nature of POSS-SC_{16} NP, which contains no π-electron and it is insulating internally (composed by polyhedral silicon oxide Si_8O_{12}) and externally (eight hexadecanthiolethyl saturated sulfur-containing hydrocarbon chains). Consistent with its current–voltage characteristic shown in Fig. 14a, POSS-SC_{16}- containing OPV exhibits the least rising slope of the current density in the neighborhood of V_{OC}, i.e., the photocurrent of OPV having the largest series resistant (R_S). However, the wide band-gap energy and charge insulating POSS-SC_{16} NP has relatively high V_{OC} and FF compared with other NPs. These make POSS-SC_{16} NP not the worst one among NP-containing OPVs. On the other hand, the conducting nature of metallic Au-SC_{12} NP does not seem to help much for P3HT/PCBM OPV, which has been proven recently by other research groups [38]. Our acquired dark current (at reverse bias in Fig. 14(b)) of Au-SC_{12}-containing OPV is the largest among all OPVs with or without NPs. Such dark current characteristic of Au-SC_{12} NP makes its OPVs relatively small V_{OC} and FF (Table 1). When increasing the NP dopant concentration to 5 wt%, V_{OC} and FF of Au-SC_{12}-containing OPV worsen further and become the smallest among all. Among all semiconducting NPs, CdS-SPh NP is the only one with charge transporting aromatic surface capping agent and it behaves the best for P3HT/PCBM OPVs. It has the highest J_{SC}, V_{OC}, FF, and hence PCE of 3.91%, only slightly lower than 4.01% of P3HT/PCBM control device. Although PbS-OA NP has the advantage of near-IR absorption and properly aligned LUMO energy level (relative to that of P3HT), the contribution to the absorption of sunlight is too little and the charge insulating surface capping agent limits the electron transfer from P3HT and the charge transporting between each PbS-OA NP. Disadvantageously, PbS-OA-containing OPVs show the second highest dark current among all devices (Fig. 14(b)), which is part of the reason for its worst V_{OC} and FF, and hence the poorest PCE (Table 1).

Similarly for 3 wt% CdS-SC_{12} NP device, good PCE (mainly due to high J_{SC}) of CdS-SPh NP device is shown in its high photocurrent (Fig. 15(a)). Both CdS-SC_{12} and CdS-SPh NP devices have even higher photocurrent at visible wavelength, particularly 400–650 nm where P3HT strongly absorbs but PCBM weakly absorbs or does not absorb, when compared to the P3HT/PCBM control device. Since either CdS-SC_{12} or CdS-SPh NP makes little contribution in the light harvesting of P3HT/PCBM bulk heterojunction device (see Figs. 8 and 15d), the high photocurrent should be attributed to the good P3HT exciton diffusion, efficient charge separation of P3HT exciton, and efficient hole and electron transporting in the P3HT/PCBM/NP hybrid system. Based on our energy level determination in this study (Fig. 10), we have demonstrated that electron transfer between P3HT and CdS-SC_{12} is unlikely and that between P3HT and CdS-SPh is highly questionable. Moreover, based on our TOF charge mobility measurement of P3HT/PCBM and P3HT/PCBM CdS-SPh hybrid systems (Fig. 13), CdS-SPh NP shows the characteristic of improving both hole and electron mobility of P3HT/PCBM. Considering the surface capping organics of CdS-SC_{12} NP are charge insulating, we may conclude that semiconducting CdS-SPh NP may be the best choice in the present study to improve the exciton diffusion and to facilitate the charge transporting of P3HT/PCBM blends.

Accordingly, in our second set of BHJ P3HT/PCBM OPV testing, CdS-SPh NP was chosen to blend in with P3HT/PCBM but the composition of PCBM was proportionally reduced. In other words, we intend to test the viability of replacing PCBM with CdS-SPh NP as the electron acceptor in the polymer–inorganic hybrid BHJ OPVs. In addition to the EQE spectra, current density vs. voltage

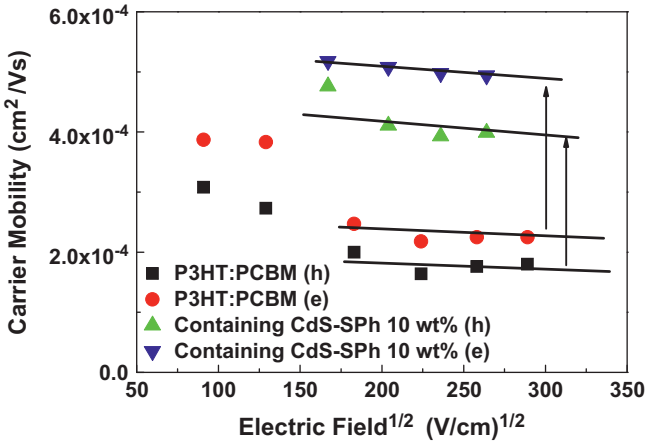

Fig. 13. TOF-determined charge carrier mobility of P3HT/PCBM with or without CdS-SPh NP dopant (10 wt%).

Table 1
Performance of P3HT/PCBM OPVs containing various NP dopants (3 and 5 wt%).

Device and NP dopant	J_{SC} (mA/cm²)	V_{OC} (V)	FF (%)	PCE (%)
P3HT/PCBM Reference	9.60	0.63	66.4	4.01
POSS-SC_{16} 3 wt% (5 wt%)	9.19(8.70)	0.62(0.61)	62.7(65.1)	3.57(3.45)
CdS-SC_{12} 3 wt% (5 wt%)	10.05(9.36)	0.60(0.59)	60.8(60.0)	3.67(3.31)
CdS-SPh 3 wt% (5 wt%)	10.07(9.91)	0.62(0.61)	62.7(63.8)	3.91(3.86)
PbS-OA 3 wt% (5 wt%)	9.66(9.10)	0.59(0.58)	58.3(56.5)	3.32(2.99)
Au-SC_{12} 3 wt% (5 wt%)	9.74(9.40)	0.58(0.57)	59.7(56.4)	3.38(3.03)

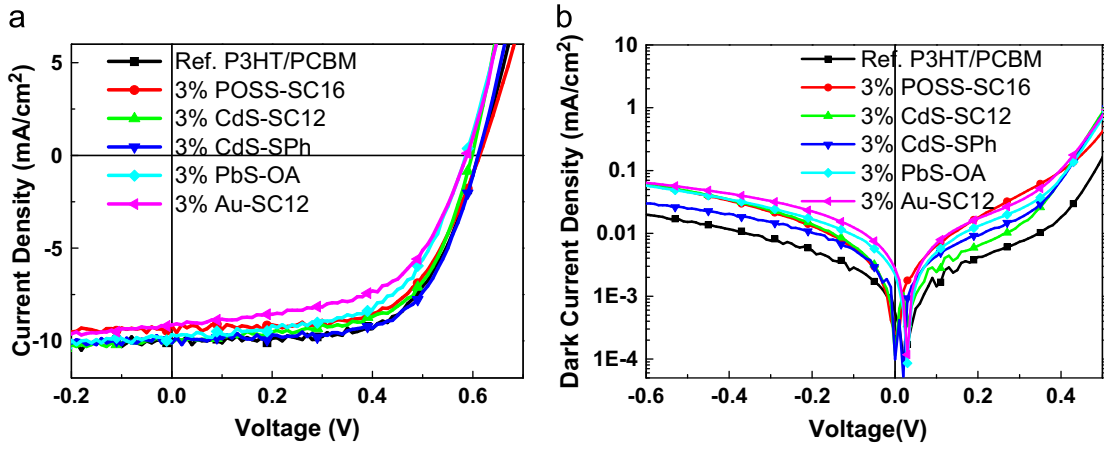

Fig. 14. Current density vs voltage characteristics of P3HT/PCBM OPVs containing various NP dopants (3 wt%): (a) under 100 mW/cm² AM1.5 illumination, and (b) in the dark.

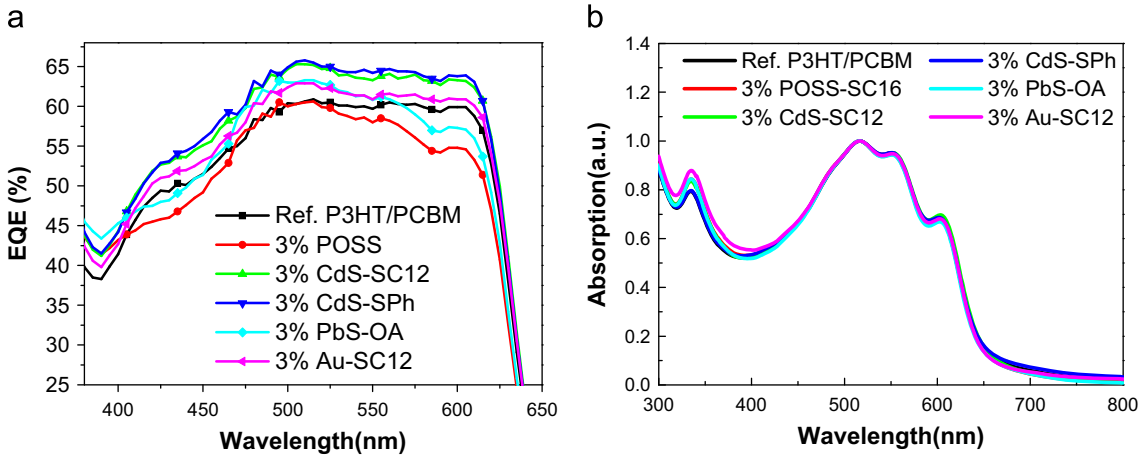

Fig. 15. (a) Wavelength dependent photocurrent of P3HT/PCBM OPVs containing various NP dopants (3 wt%). (b) Wavelength dependent light absorption intensity (normalized at 516 nm) of P3HT/PCBM thin films containing various NP dopants (3 wt%) spin-coated on PEDOT:PSS ITO glass substrate.

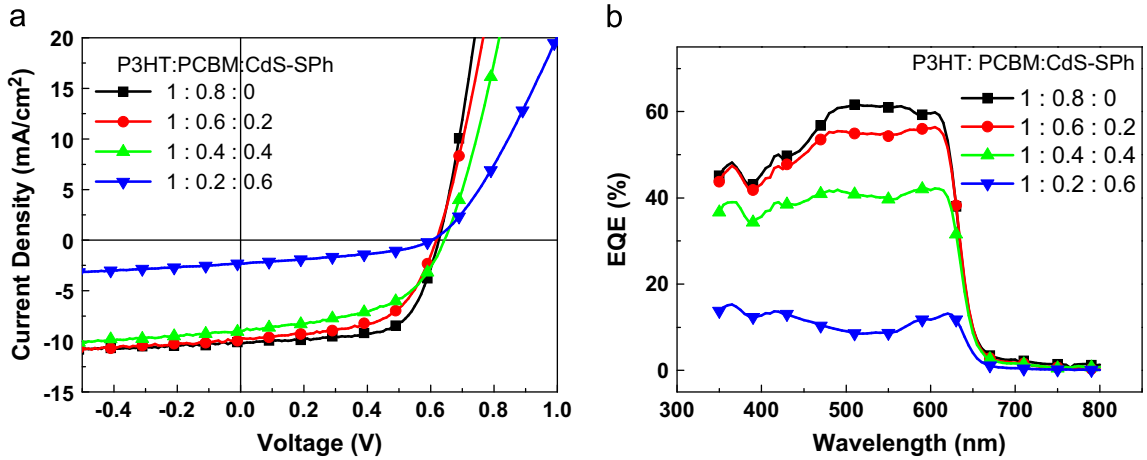

Fig. 16. (a) Current density vs voltage characteristics of P3HT/PCBM/CdS-SPh OPVs with variable composition ratios. (b) EQE spectra of the same set of OPVs.

Table 2
Performance of P3HT/PCBM/CdS-SPh OPV with variant composition weight ratios.

Composition weight ratio of P3HT/PCBM/CdS-SPh	J_{SC} (mA/cm^2)	V_{OC} (V)	FF (%)	PCE (%)	R_{SH} (Ω/cm^2)	R_S (Ω/cm^2)
1: 0.8: 0	10.2	0.63	64	4.14	730	3.7
1: 0.6: 0.2	9.7	0.62	59	3.52	380	4.7
1: 0.4: 0.4	9.0	0.65	51	2.97	320	5.7
1: 0.2: 0.6	2.3	0.61	39	0.55	290	15.7

characteristics of OPVs with variable composition ratios are shown in Fig. 16. Data of the OPV performance are summarized in Table 2.

As clearly shown in the results of P3HT/PCBM/CdS-SPh OPV, the performance in all aspects (J_{SC}, V_{OC}, FF, R_{SH}, R_S, and PCE) starts deteriorating once the replacement of PCBM by CdS-SPh takes place and it is getting worse with increasing composition ratio between PCBM and CdS-SPh, from 3 to 1, 1 to 1, and 1 to 3 (Table 2). Such results also mean that PCBM is a far better electron acceptor material than CdS-SPh NP for P3HT-based BHJ OPVs. One thing worth noting is the poor solubility of CdS-SPh NP in 1,2-dichlorobenzene, the solvent we used for solution process in the fabrication of P3HT/PCBM/NP thin film. There are noticeable amounts of CdS-SPh NPs remaining insoluble (in the formation of agglomeration and/or aggregation) in the prepared solution. In order to keep the required composition ratio of CdS-SPh NP, we have to omit the filtration process and take the 1,2-dichlorobenzene solution for spin-coating directly. Therefore, it is conceivable that a significant amount of NP agglomeration and/or aggregation exists in the thin film of the high ratio CdS-SPh NP-containing P3HT/PCBM OPV. In addition to the less suitable LUMO energy level alignment with P3HT, more serious agglomeration and/or aggregation than that of PCBM is another adverse effect of CdS-SPh NP applied in the hybrid polymer-based BHJ OPVs.

4. Conclusions

For the first time, we have a unified investigation on six kinds of NPs blending with P3HT/PCBM for the solution process fabrication of hybrid BHJ OPVs. Several insightful physical and chemical properties of these NPs have been acquired from the study. Regardless of the conductivity content (conducting, semiconducting, or insulating) and sunlight absorption (transparent, visible or near-IR absorbing), the NP hybrid P3HT/PCBM OPVs show no sign of PCE improvement. Conclusively from our spectroscopic and physical studies, some of these NPs (POSS-SC16, CdS-SC$_{12}$, PbS-OA, and Au-SC12) have charge or electron transfer blocking surface capping agent and cannot intimately contact with electron donor material P3HT. For CdS-SPh and Au-SPh NPs, charge conducting surface capping thiophenol causes insufficient solubility of the NPs and serious agglomeration and/or aggregation in the thin film of P3HT/PCBM, of which the charge or electron transferring contact between P3HT and NPs is significantly limited. Regarding energy

level alignment of P3HT and NP, LUMO energy offset or work function energy is fine for PbS-OA and Au-SC_{12} NP, respectively, whereas it is beyond the range for POSS-SC_{16} NP. However, their insulating surface capping agents prevent the charge or electron transfer from P3HT. For CdS-SPh NPs, its LUMO energy level is higher than that of P3HT and the charge separation of P3HT exciton is unlikely. PbS-OA or Au-SC_{12} NP has the advantage of near-IR and visible light absorption but its absorbance is too low to make a practical contribution when compared with that of P3HT in the hybrid OPVs. Little enhancing effect, if it is observed experimentally, was found for these NPs on the stacking of P3HT polymer chains. The enhancement of sunlight harvesting of P3HT by NPs hybrid does not seem feasible either.

Conclusively from the present study, NPs viable for enhancing PCE of P3HT/PCBM BHJ OPVs should meet the following criteria. First, NPs should be appropriate in LUMO energy offset (with P3HT). Second, NPs should be surface-capped with charge transporting agent. Third, NPs should be well dispersed in P3HT/PCBM system. Fourth, the content of the NPs should perhaps be semiconducting or conducting. Light absorption or long wavelength absorption of NPs is not a necessary option in the P3HT/PCBM system, unless its absorbance is comparable with or stronger than that of polymer or fullerene in the system. Unfortunately, we note that it is a potential conflict between the second and third criteria, regarding surface capping agent. Finally, as mentioned by one of the reviewers, surfactant assisted NP dispersion approach has been utilized in aqueous processing of OPV roll-to-roll printing [72]. Such an NP dispersion method might be useful in controlling the agglomeration and/or aggregation of the NP in P3HT/PCBM blends.

Acknowledgments

This research was supported in part by the National Science Council of Taiwan (Grant nos. NSC 98-2119-M-001-026 and 97-2628-M-001-014-MY3), the Nanoscience and Nanotechnology Research Program of Academia Sinica, and the Institute of Chemistry of Academia Sinica. We thank Prof. Li-Chyong Chen of National Taiwan University for her kind assistance in SEM and EDS measurements.

References

[1] C.J. Brabec, J.A. Hauch, P. Schilinsky, C. Waldauf, Production aspects of organic photovoltaics and their impact on the commercialization of devices, MRS Bulletin 30 (2005) 50–52.
[2] M. Manceau, D. Angmo, M. Jørgensen, F.C. Krebs, ITO-free flexible polymer solar cells: from small model devices to roll-to-roll processed large modules, Organic Electronics 12 (2011) 566–574.
[3] R. Søndergaard, M. Hösel, D. Angmo, T.T. Larsen-Olsen, F.C. Krebs, Roll-to-roll fabrication of polymer solar cells, Materials Today 15 (2012) 36–49.
[4] W. Ma, C. Yang, X. Gong, K. Lee, A.J. Heeger, Thermally stable, efficient polymer solar cells with nanoscale control of the interpenetrating network morphology, Advanced Functional Materials 15 (2005) 1617–1622.
[5] B.C. Thompson, J.M. Fréchet, Polymer–fullerene composite solar cells, Angewandte Chemie International Edition 47 (2008) 58–77.
[6] Y.-J. Cheng, S.-H. Yang, C.-S. Hsu, Synthesis of conjugated polymers for organic solar cell applications, Chemical Reviews 109 (2009) 5868–5923.
[7] Y. Liang, L. Yu, Development of semiconducting polymers for solar energy harvesting, Polymer Reviews 50 (2010) 454–473.
[8] R.F. Service, Outlook brightens for plastic solar cells, Science 332 (2011) 293 pp.
[9] Z. He, C. Zhong, X. Huang, W.-Y. Wong, H. Wu, L. Chen, S. Su, Y. Cao, Simultaneous enhancement of open-circuit voltage, short-circuit current density, and fill factor in polymer solar cells, Advanced Materials 23 (2011) 4636–4643.
[10] Y. Li, Molecular design of photovoltaic materials for polymer solar cells: toward suitable electronic energy levels and broad absorption, Account of Chemical Research 45 (2012) 723–733.
[11] H.-L. Yip, A.K.-Y. Jen, Recent advances in solution-processed interfacial materials for efficient and stable polymer solar cells, Energy & Environmental Science 5 (2012) 5994–6011.
[12] H.J. Son, B. Carsten, I.H. Jung, L. Yu, Overcoming efficiency challenges in organic solar cells: rational development of conjugated polymers, Energy & Environmental Science 5 (2012) 8158–8170.
[13] R.L. Uy, S.C. Price, W. You, Structure-property optimizations in donor polymers via electronics, substituents, and side chains toward high efficiency solar cells, Macromolecular Rapid Communications 33 (2012) 1162–1177.
[14] G. Li, R. Zhu, Y. Yang, Polymer solar cells, Nature Photonics 6 (2012) 153–161.
[15] L. Dou, J. You, J. Yang, C.-C. Chen, Y. He, S. Murase, T. Moriarty, K. Emery, G. Li, Y. Yang, Tandem polymer solar cells featuring a spectrally matched low-bandgap polymer, Nature Photonics 6 (2012) 180–185.
[16] X. Li, W.C.H. Choy, L. Huo, F. Xie, W.E.I. Sha, B. Ding, X. Guo, Y. Li, J. Hou, J. You, Y. Yang, Dual plasmonic nanostructures for high performance inverted organic solar cells, Advanced Materials 24 (2012) 3046–3052.
[17] L. Dou, J. Gao, E. Richard, J. You, C.-C. Chen, K.C. Cha, Y. He, G. Li, Y. Yang, Systematic investigation of benzodithiophene- and diketopyrrolopyrrole-based low-bandgap polymers designed for single junction and tandem polymer solar cells, Journal of the American Chemical Society 134 (2012) 10071–10079.
[18] Z. He, C. Zhong, S. Su, M. Xu, H. Wu, Y. Cao, Enhanced power-conversion efficiency in polymer solar cells using an inverted device structure, Nature Photonics 6 (2012) 591–595.
[19] F. Padinger, R.S. Rittberger, N.S. Sariciftci, Effects of postproduction treatment on plastic solar cells, Advanced Functional Materials 13 (2003) 85–88.
[20] T. Erb, U. Zhokhavets, G. Gobsch, S. Raleva, B. Stuhn, P. Schilinsky, C. Waldauf, C.J. Brabec, Correlation between structural and optical properties of composite polymer/fullerene films for organic solar cells, Advanced Functional Materials 15 (2005) 1193–1196.
[21] G. Li, V. Shrotriya, J. Huang, Y. Yao, T. Moriarty, K. Emery, Y. Yang, High-efficiency solution processable polymer photovoltaic cells by self-organization of polymer blends, Nature Materials 4 (2005) 864–868.
[22] G. Li, Y. Yao, H. Yang, V. Shrotriya, G. Yang, Y. Yang, "Solvent annealing" effect in polymer solar cells based on poly93-hexylthiophene) and methanofullerences, Advanced Functional Materials 17 (2007) 1636–1644.
[23] X. Yang, J. Loos, S.C. Veenstra, W.J.H. Verhees, M.M. Wienk, J.M. Kroon, M.A.J. Michels, R.A.J. Janssen, Nanoscale morphology of high-performance polymer solar cells, Nano Letters 5 (2005) 579–583.
[24] H. Hoppe, N.S. Sariciftci, Morphology of polymer/fullerene bulk heterojunction solar cells, Journal of Materials Chemistry 16 (2006) 45–61.
[25] W. Chen, M.P. Nikiforov, S.B. Darling, Morphology characterization in organic and hybrid solar cells, Energy Environmental Science 5 (2012) 8045–8074.
[26] S. Günes, N.S. Sariciftci, Hybrid solar cells, Inorganic Chimica Acta 361 (2008) 581–588.
[27] P.-L. Ong, I.A. Levitsky, Organic/IV, III–V semiconductor hybrid solar cells, Energies 3 (2010) 313–334.
[28] T. Song, S.-T. Lee, B. Sun, Prospects and challenges of organic/group IV nanomaterial solar cells, Journal of Materials Chemistry 22 (2012) 4216–4232.
[29] M. Helgesen, R. Søndergaard, F.C. Krebs, Advanced materials and processes for polymer solar cell devices, Journal of Materials Chemistry 20 (2010) 36–60.
[30] J. Chandrasekaran, D. Nithyaprakash, K.B. Ajjan, S. Maruthamuthu, D. Manoharan, S. Kumar, Hybrid solar cell based on blending of organic and inorganic materials—an overview, Renewable Sustainable Energy Reviews 15 (2011) 1228–1238.
[31] B.R. Saunders, M.L. Turner, Nanoparticle-polymer photovoltaic cells, Advances in Colloid Interface Science 138 (2008) 1–23, and references cited therein.
[32] K.M. Coakley, Y. Liu, C. Goh, M.D. McGehee, Ordered organic–inorganic bulk heterojunction photovoltaic cells, MRS Bulletin 30 (2005) 37–40.
[33] K.M. Coakley, Y. Liu, M.D. McGehee, K.L. Frindell, G.D. Stucky, Infiltrating semiconducting polymers into self-assembled mesoporous titania films for photovoltaic applications, Advanced Functional Materials 13 (2003) 301–306.
[34] G.P. Bartholomew, A.J. Heeger, Infiltration of regioregular poly[2,2′-(3-hexylthiophene)] into random nanocrystalline TiO_2 networks, Advanced Functional Materials 16 (2005) 677–682.
[35] K.J. Jiang, K. Manseki, Y.H. Yu, N. Masaki, K. Suzuki, Y.L. Song, S. Yanagida, Photovoltaics based on hybridization of effective dye-sensitized titanium oxide and hole-conductive polymer P3HT, Advanced Functional Materials 19 (2009) 2481–2485.
[36] M.-Y. Chang, Y.-F. Chen, Y.-S. Tsai, K.-M. Chi, Blending platinium nanoparticles into poly(3-hexylthiophene):[6,6]-phenyl-C61-butyric acid methyl ester enhances the efficiency of polymer solar cells, Journal of the Electrochemical Society 156 (2009) B234–B237.
[37] V.K. Naidu, J.S. Park, S.C. Kim, S.-M. Park, E.-J. Lee, K.-J. Yoon, S.J. Lee, J.W. Lee, Y.-S. Gal, S.-H. Jin, Novel hybrid polymer photovoltaics made by generating silver nanoparticles in polymer:fullerene bulk-heterojunction structures, Solar Energy Materials and Solar Cells 92 (2008) 397–401.
[38] K. Topp, H. Borchert, F. Johnen, A.V. Tunc, M. Knipper, E. von Hauff, J. Parisi, K. Al-Shamery, Impact of the incorporation of Au nanoparticles into polymer/fullerene solar cells, Journal of Physical Chemistry A 114 (2010) 3981–3989.
[39] K. Kim, D.L. Carroll, Roles of Au and Ag nanoparticles in efficiency enhancement of poly(3-octylthiophene)/C60 bulk heterojunction photovoltaic devices, Applied Physics Letters 87 (2005) 203113–203113-3.
[40] M.T. Khan, R. Bhargav, A. Kaure, S.K. Dhawan, S. Chand, Effect of cadmium sulphide quantum dot processing and post thermal annealing on P3HT/PCBM photovoltaic device, Thin Solid Films 519 (2010) 1007–1011.

[41] D. Jarzab, K. Szendrei, M. Yarema, S. Pichler, W. Heiss, M.A. Loi, Charge-separation dynamics in inorganic-organic ternary blends for efficient infrared photodiodes, Advanced Functional Materials 21 (2011) 1988–1992.
[42] H.-Y. Chen, M.K.F. Lo, G. Yang, H.G. Monbouquette, Y. Yang, Nanoparticle-assisted high photoconductive gain in composites of polymer and fullerene, Nature Nanotechnology 3 (2008) 543–547.
[43] S.-W. Liu, J.-H. Lee, C.-C. Lee, C.-T. Chen, J.-K. Wang, Charge carrier mobility of mixed-layer organic light-emitting diodes, Applied Physics Letters 91 (2007) 142106-1–142106-3.
[44] M.-F. Wu, S.-J. Yeh, C.-T. Chen, H. Murayama, T. Tsuboi, W.-S. Li, I. Chao, S.-W. Liu, J.-K. Wang, The quest for high-performance host materials for electrophosphorescent blue dopants, Advanced Functional Materials 17 (2007) 1887–1895.
[45] M. Brust, M. Walker, D. Bethell, D.J. Schiffrin, R. Whyman, Synthesis of thio-derivatised gold nanoparticles in a two-phase liquid-liquid system, Journal of the Chemical Society, Chemical Communications (1994) 801–802.
[46] M.A. Hines, G.D. Scholes, Colloidal PbS nanocrystals with size-tunable near-infrared emission: observation of post-synthesis self-narrowing of the particle size distribution, Advanced Materials 15 (2003) 1844–1849.
[47] A. Agostiano, M. Catalano, M.L. Curri, M.D. Monica, L. Manna, L. Vasanelli, Synthesis and structural characterisation of CdS nanoparticles prepared in a four-components “water-in-oil” microemulsion, Micron 31 (2000) 253–258.
[48] N. Herron, Y. Wang, H. Eckert, Synthesis and characterization of surface-capped, size-quantied CdS clusters. Chemical control of cluster size, Journal of the American Chemical Society 112 (1990) 1322–1326.
[49] H. Xu, B. Yang, X. Gao, C. Li, S. Guang, Synthesis and characterization of organic–inorganic hybrid polymers with a well-defined structure from diamines and epoxy-functionalized polyhedral oligomeric silsesquioxanes, Journal of Applied Polymer Science 101 (2006) 3730–3735.
[50] J. Choi, J. Harcup, A.F. Yee, Q. Zhu, R.M. Laine, Organic/inorganic hybrid composites from cubic silsesquioxanes, Journal of the American Chemical Society 123 (2001) 11420–11430.
[51] C.-M. Leu, G.M. Reddy, K.-H. Wei, C.-F. Shu, Synthesis and dielectric properties of polyimide-chain-end tethered polyhedral oligomeric silsesquioxane nanocomposites, Chemistry of Materials 15 (2003) 2261–2265.
[52] C.-H. Lu, S.-W. Kuo, C.-F. Huang, F.-C. Chang, Self-assembled fernlike microstructures of polyhedral oligomeric silsesquioxane/gold nanoparticle hybrids, Journal of Physical Chemistry C 113 (2009) 3517–3524.
[53] J. Wu, P.T. Mather, POSS polymers: physical properties and biomaterials applications, Polymer Reviews 49 (2009) 25–63.
[54] W.Y. Huang, C.C. Lee, S.G. Wang, Y.K. Han, M.Y. Chang, Side chain effects of poly(3-alkylthiophene) on the morphology and performance of polymer solar cells, Journal of the Electrochemical Society 157 (2010) B1336–B1342.
[55] Y.-H. Chen, P.-T. Huang, K.-C. Lin, Y.-J. Huang, C.-T. Chen, Stabilization of poly (3-hexylthiophene)/PCBM morphology by hydroxyl group end-functionalized P3HT and its application to polymer solar cells, Organic Electronics 13 (2012) 283–289.
[56] L.H. Nguyen, H. Hoppe, T. Erb, S. Günes, G. Gobsch, N.S. Sariciftci, Effects of annealing on the nanomorphology and performance of poly(alkylthiophene): fullerene bulk-heterojunction solar cells, Advanced Functional Materials 17 (2007) 1071–1078.
[57] M. Campoy-Quiles, T. Ferenczi, T. Agostinelli, P.G. Etchegoin, Y. Kim, T.D. Anthopoulos, P.N. Stavrinou, D.D.C. Bradley, A.J. Nelson, Morphology evolution via self-organization and lateral and vertical diffusion in polymer: fullerene solar cell blends, Nature Materials 7 (2008) 158–164.
[58] A.M. Ballantyne, T. Ferenczi, M. Campoy-Quiles, T.M. Clarke, A. Maurano, K. H. Wong, W. Zhang, N. Stingelin-Stutzmann, J.-S. Kim, D.D.C. Bradley, J.R. Durrant, I. McCulloch, M. Heeney, J. Nelson, S. Tierney, W. Duffy, C. Mueller, P. Smith, Understanding the influence of morphology on poly(3-hexylselenothiophene):PCBM solar cells, Macromolecules 43 (2010) 1169–1174.
[59] A. Swinnen, I. Haeldermans, M. vande Ven, J. D'Haen, G. Vanhoyland, S. Aresu, M. D'Olieslaeger, J. Manca, Tuning the dimensions of C60-based needlelike crystals in blended thin films, Advanced Functional Materials 16 (2006) 760–765.
[60] P. Anderson, Work function of gold, Physical Review 115 (1959) 553–554.
[61] K. Hong, J.W. Lee, S.Y. Yang, K. Shin, H. Jeon, S.H. Kim, C. Yang, C.E. Park, Lower hole-injection barrier between pentacene and a 1-hexadecanethiol-modified gold substrate with a lowered work function, Organic Electronics 9 (2008) 21–29.
[62] S.-H. Lee, W.-C. Lin, C.-J. Chang, C.-C. Huang, C.-P. Liu, C.-H. Kuo, H.-Y. Chang, Y.-W. You, W.-L. Kao, G.-J. Yen, D.-Y. Kuo, Y.-T. Kuo, M.-H. Tsai, J.-J. Shyue, Effect of the chemical composition on the work function of gold substrates modified by binary self-assembled monolayers, Physical Chemistry and Chemical Physics 13 (2011) 4335–4339.
[63] N. Zhao, T.P. Osedach, L.-Y. Chang, S.M. Geyer, D. Wanger, M.T. Binda, A.C. Arango, M.G. Bawendi, V. Bulovic, Colloidal PbS quantum dot solar cells with high fill factor, ACS Nano 4 (2010) 3743–3752.
[64] T.M. Aita, K. Iha, L. Hui, T. Higuchi, S. Sato, Photoconductivity of n-type semiconductor nanoparticle-doped poly(N-vinylcarbazole) films, Journal of Materials Science 42 (2007) 6279–6286.
[65] Z.-L. Guan, J.B. Kim, H. Wang, C. Jaye, D.A. Fischer, Y.-L. Loo, A. Kahn, Direct determination of the electronic structure of the poly(3-hexylthiophene): phenyl-[6,6]-C61 butyric acid methyl ester blend, Organic Electronics 11 (2010) 1779–1785.
[66] C. Deibel, D. Mack, J. Gorenflot, A. Scholl, S. Krause, F. Reinert, D. Rauh, V. Dyakonov, Energetics of excited states in the conjugated polymer poly(3-hexylthiophene), Physical Review B 81 (2010) 085202–085205-5.
[67] N.C. Greenham, X. Peng, A.P. Alivisatos, Charge separation and transport in conjugated-polymer/semiconductor-nanocrystal composites studied by photoluminescence quenching and photoconductivity, Physical Review B 54 (1996) 17628–17637.
[68] M. Pientka, V. Dyakonov, D. Meissner, A. Rogach, D. Talapin, H. Weller, L. Lutsen, D. Vanderzande, Photoinduced charge transfer in composites of conjugated polymers and semiconductor nanocrystals, Nanotechnology 15 (2004) 163–170.
[69] J.N. de Freitas, I.R. Grova, L.C. Akcelrud, E. Arici, N.S. Sariciftci, A.F. Nogueira, The effects of CdSe incorporation into bulk heterojunction solar cells, Journal of Materials Chemistry 20 (2010) 4845–4853.
[70] S.S. Kawar, B.H. Pawar, Synthesis and characterization of CdS n-type of semiconductor thin films having nanometer grain size, Chalcogenide Letters 6 (2009) 219–225.
[71] K.R. Choudhury, K. Samoc, A. Patra, P.N. Prasad, Charge carrier transport in poly(*N*-vinylcarbazole):CdS quantum dot hybrid nanocomposite, Journal of Physical Chemistry B 108 (2004) 1556–1562.
[72] T.R. Andersen, T.T. Larsen-Olsen, B. Andreasen, A.P.L. Böttiger, J.E. Carlé, M. Helgesen, E. Bundgaard, K. Norrman, J.W. Andreasen, M. Jørgensen, F.C. Krebs, Aqueous processing of low-band-gap polymer solar cells using -to-roll methods, ACS Nano 5 (2011) 4188–4196.